Technical Report No. 32-415

Convective Heat Transfer in a Convergent–Divergent Nozzle

L. H. Back
P. F. Massier
H. L. Gier

JET PROPULSION LABORATORY
CALIFORNIA INSTITUTE OF TECHNOLOGY
PASADENA, CALIFORNIA

November 15, 1963

Technical Report No. 32-415

Convective Heat Transfer in a Convergent–Divergent Nozzle

L. H. Back,
P. F. Massier, and
H. L. Gier

15 Nov. 1963 35p refs

[2]

(NASA Contract NAS7-100)

(NASA CR-55317, JPL-TR-32-415) OTS: $3.6
$1.2

[x] OTS

D. R. Bartz, Chief
Propulsion Research Section

JET PROPULSION LABORATORY
CALIFORNIA INSTITUTE OF TECHNOLOGY
PASADENA, CALIFORNIA

November 15, 1963

Prepared Under Contract No. NAS 7-100
National Aeronautics & Space Administration

CONTENTS

FIGURES

FIGURES (Cont'd)

PREFACE

Portions of this paper were originated under studies conducted for the Department of Army Ordnance Corps under Contract No. DA-04-495-Ord-18. Such studies are now conducted for the National Aeronautics and Space Administration under Contract No. NAS 7-100.

13936

ABSTRACT

The results of an experimental investigation of convective heat transfer from turbulent boundary layers accelerated under the influence of large pressure gradients in a cooled convergent–divergent conical nozzle are presented. The investigation covered a range of stagnation pressures from 30 to 250 psia, stagnation temperatures from 1030 to 2000°R, and nozzle-inlet boundary-layer thicknesses between 5 and 25% of the inlet radius. Steady-state heat-transfer rates from air heated by the combustion of methanol were determined locally from measurements using thermocouples embedded in the nozzle wall. The most significant unexpected trend in the results is the reduction in the heat-transfer coefficient, below the variation with stagnation pressure anticipated for a turbulent boundary layer, at stagnation pressures less than about 75 psia. As expected, the results include a maximum in the heat-transfer coefficient upstream of the throat, where the mass flow rate per unit area is largest, and a substantial decrease of the heat-transfer coefficient downstream of the point of flow separation, which occurred in the divergent section of the nozzle at the low stagnation pressures. A reduction of about 10% in the heat-transfer coefficient resulted from an increase in the inlet boundary-layer thickness between the minimum and maximum thicknesses investigated.

Heat-transfer predictions with which the data were compared either incorporate a prediction of the boundary-layer characteristics or are related to pipe flow. At the higher stagnation pressures, predicted values from a modification of Bartz' turbulent boundary-layer analysis are in fair agreement with the data. As a possible explanation of the low heat-transfer rates at the lower stagnation pressures, a parameter is found which is a measure of the importance of flow acceleration in reducing the turbulent transport below that typical of a fully turbulent boundary layer.

AUTHOR

I. INTRODUCTION

Comprehensive studies of convective heat transfer from gases flowing under the influence of comparatively large pressure gradients have been mostly analytical. Laminar flow cases have been solved by boundary-layer theory approaches in which the restrictive assumptions are within the realm of describing actual processes. Turbulent flows, however, are too complex to formulate in such a way that descriptions of the momentum and energy transport processes can be made without the use of considerable empirical information or assumptions which are so drastic that they themselves are essentially the solutions. The present investigation was undertaken in order to provide experimental convective heat-transfer information on turbulent flows subjected to large pressure gradients with boundary layers that are thin in comparison to the cross section of the channels. It was anticipated that these results could be incorporated with turbulent boundary-layer theories to arrive at a meaningful method of predicting convective heat transfer in accelerating flows.

Experimental measurements of heat transfer from gases flowing under the influence of pressure gradients have been made to some extent by other investigators. Data obtained from rocket-engine firings indicate that the local heat fluxes in nozzles (particularly the convergent sections) are sensitive to injection schemes, combustion phenomena, and the proximity of a nozzle to the injector (Ref. 1). Furthermore, superimposed on the convective component is a radiation component, which, together with the other effects, introduces complexities into the gross heat-transfer process. Hence, results of measurements such as these have not been particularly informative about the convective heat-transfer mechanism in accelerating turbulent boundary-layer flows.

Most experimental results of previous investigations of convective heat transfer in a nozzle without injection and combustion effects were obtained either with nozzles of small angles of convergence and divergence or at relatively low stagnation pressures and temperatures. Saunders and Calder's measurements (Ref. 2) were made only in the conical divergent section, with the half-angle of divergence about ½ deg. Ragsdale and Smith (Ref. 3) using superheated steam, made measurements in a nozzle which had small convergent and divergent half-angles of about 1 deg. The stagnation temperature was about 1000°R, and the stagnation pressure ranged from 20 to 35 psia. Baron and Durgin's measurements (Ref. 4) in two-dimensional nozzles were made at a stagnation temperature of 570°R and over a stagnation pressure range of 6 to 30 psia. In preliminary results (Ref. 5), from the system shown in Fig. 1, semilocal values of heat transfer were determined by calorimetry for a few operating conditions. Only for Kolozsi's measurements (Ref. 6) in a 7½-deg half-angle convergent and divergent conical nozzle at a stagnation temperature of about 1200°R were

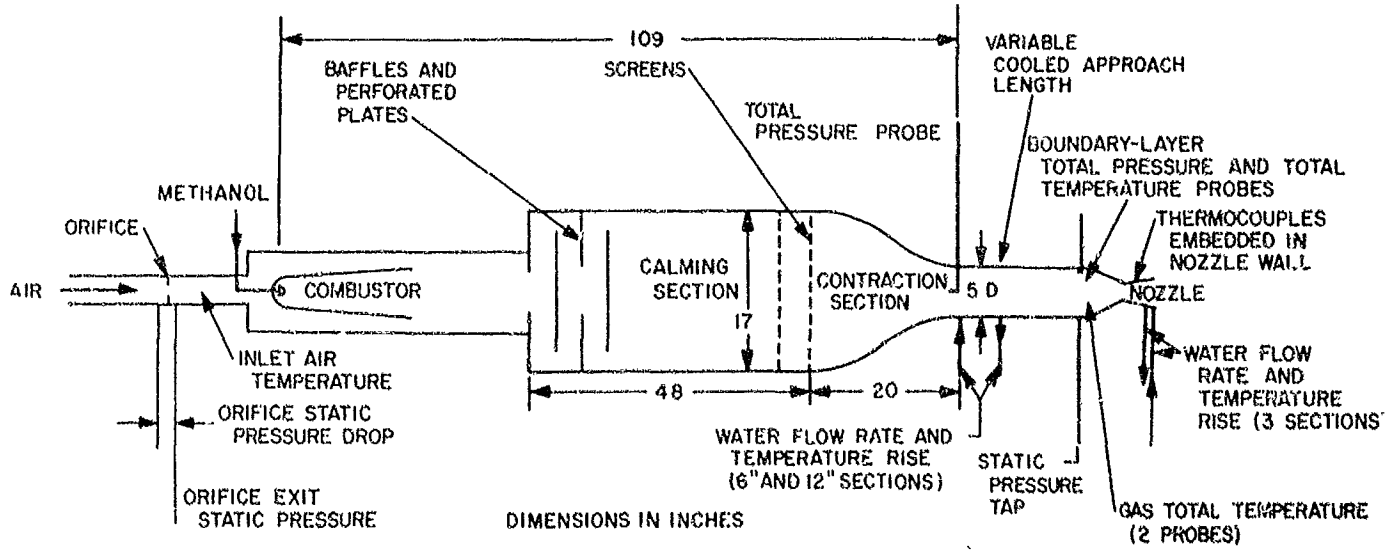

Fig. 1. Flow and instrumentation diagram

data reported at higher stagnation pressures of 225 and 370 psia.

In this investigation, which covered a range of stagnation pressures from 30 to 250 psia and stagnation temperatures from 1030 to 2000°R, compressed air was heated by the internal combustion of methanol and then mixed to obtain uniformity before it entered the nozzle. The mixing and distance of the combustion from the nozzle (Fig. 1) minimized maldistributions, and the ratio of methanol-to-air weight flow rate was small enough, even for the highest stagnation temperature, so that the products of combustion could be treated approximately as air. The nozzle had a throat diameter of 1.803 in., a contraction-area ratio of 7.75 to 1, an expansion-area ratio of 2.68 to 1, a convergent half-angle of 30 deg, and a divergent half-angle of 15 deg. The exit Mach number was about 2.5. Local convective heat-transfer results were obtained by measuring steady-state temperatures with thermocouples embedded in the water-cooled nozzle wall. Radiation effects were negligible over the stagnation-temperature range. To determine the effect of boundary-layer thickness at the nozzle inlet on heat transfer in the nozzle, the length of the constant-diameter cooled approach section upstream of the nozzle inlet was changed in 6-in. lengths from 0 to 18 in.

II. INSTRUMENTATION

The system flow and instrumentation diagram is shown in Fig. 1. Stagnation pressure was measured just upstream of the water-cooled approach section, and stagnation temperature was determined by averaging the readings of two shielded thermocouples placed 0.25 in. upstream of the nozzle inlet. These two thermocouples, located 1 in. from the centerline, were spaced 180 deg apart circumferentially and generally read within 2% of each other. To determine the static-pressure distribution along the nozzle, thirty-two static-pressure holes 0.040 in. in diameter were spaced circumferentially and axially in the nozzle wall. These static pressures were measured with mercury manometers.

Boundary-layer traverses were made in the 5.07-in.-diameter cooled approach section at a location 1.25 in. upstream of the nozzle inlet. The stagnation-pressure probe was located 90 deg circumferentially from the stagnation-temperature probe. Details of the probe tips are shown in Fig. 2. The tip design is similar to that of probes used by Livesey (Ref. 7), with which he found a

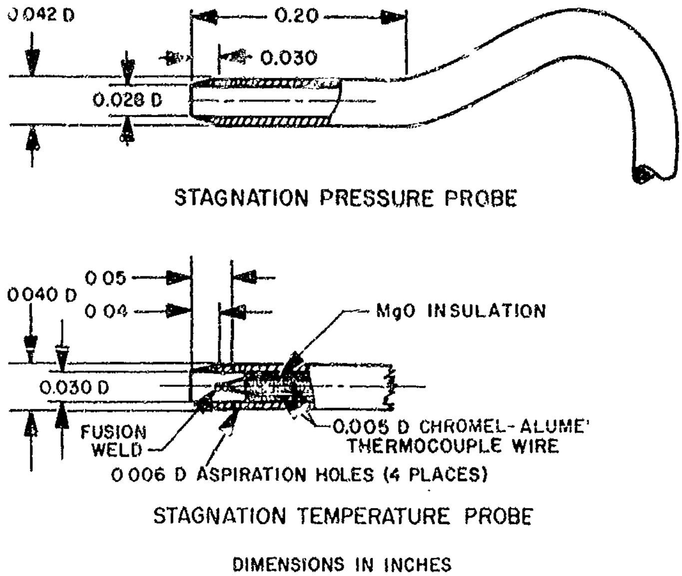

Fig. 2. Tip details of traversing boundary-layer probes

negligible velocity displacement effect of the probe in the wall vicinity. The probes were moved mechanically via a micrometer lead screw, and their location from the wall was determined by a counter and a helipot.

Steady-state wall temperatures and heat fluxes wer obtained from thermocouples embedded in cylindrica plugs, a typical one of which is shown in Fig. 3. Thre thermocouples were formed along the length of eac plug, which was pressed into a hole drilled through th nozzle wall. In the Appendix, the construction and cal bration of the plugs are described, including the deter mination of the distance between thermocouple wel junctions by means of a Kelvin bridge circuit. On thermocouple plug was located at each of twenty-on axial locations, except at $x/L = 0.864$, where there we two. These plugs were also spaced at numerous circum ferential locations along the nozzle, as indicated in th table in Fig. 3, such that every third plug was located a quadrant within 55 deg of successive ones. The nozz and plugs were fabricated from the same billet of 50 type stainless steel. Available data on the thermal co ductivity of this material indicated a small variation wit temperature in the attainable wall temperature rang Values of thermal conductivity used in the data reduc tion were obtained experimentally on material take from the same billet that was used to fabricate the nozz Three longitudinal water-coolant passages cooled t outer surface of the nozzle and plugs. The nozzle insta lation is shown in Fig. 4.

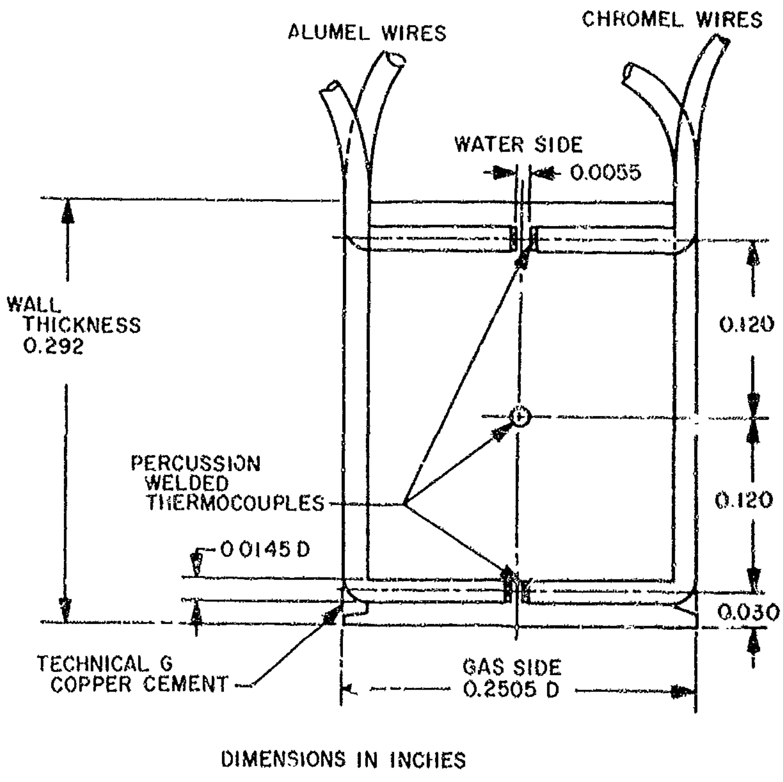

PLUG POSITION[a]			
PLUG No.	x/L	A/A*	CIRCUMFERENTIAL ANGLE FROM ARBITRARY ZERO deg
I24	0.133	6.39	330
D25	0.204	5.03	30
D34	0.276	3.86	150
I23	0.336	2.98	280
D26	0.335	2.37	80
D35	0.429	1.84	200
I22	0.46-	1.48	315
D28	0.512	1.23	45
H37[b]	0.541	1.10	135
I20[c]	0.573	1.02	300
D29	0.603	1.00	60
F42	0.634	1.07	180
I19	0.664	1.08	285
D30	0.693	1.19	75
F43	0.717	1.08	200
I18	0.730	1.41	320
D31	0.782	1.55	40
F45[c]	0.825	1.74	150
I17	0.864	1.94	275
C16	0.864	1.94	330
D33	0.905	2.14	85
F46	0.938	[illegible]	305

[a]L = 3.925 in. and A* = 2.557 in.² at x/L = 0.632.
[b]Data from this plug are questionable and have been omitted.
[c]Water side wall thermocouple in this plug has been damaged.

Fig. 3. Thermocouple plug diagram and positions

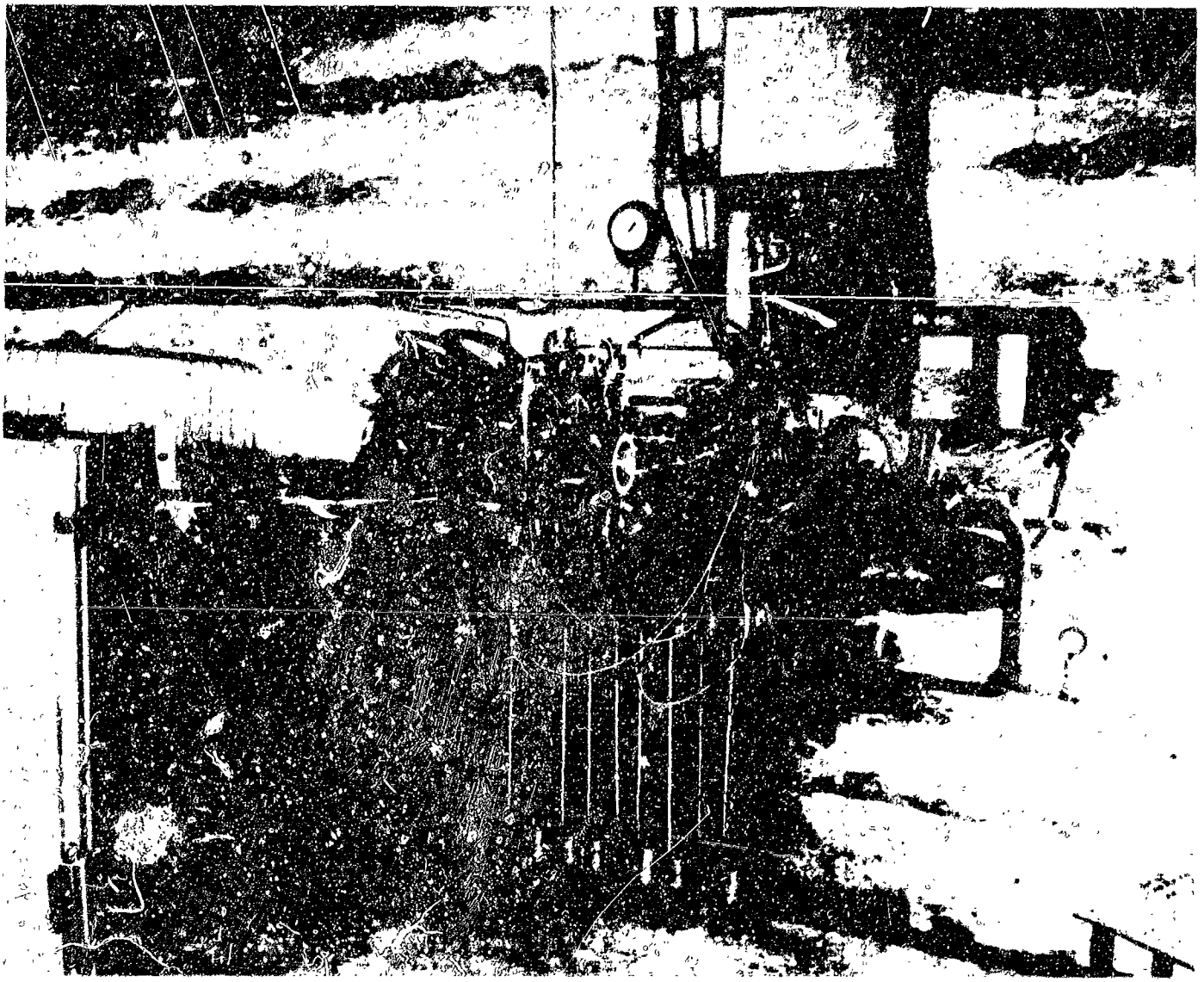

Fig. 4. Nozzle installation

III. HEAT-TRANSFER CALCULATION PROCEDURE

Although temperature gradients existed along the nozzle wall, as indicated by the wall isotherms shown in Fig. 5 for a particular test, these were generally small, and the three thermocouple readings in each plug indicated that only radial heat conduction normal to the wall need be considered. The local heat flux q_w normal to the gas-side wall was computed from

$$q_w = \frac{k(T_a - T_b)}{r_a \ln r_b/r_a} \qquad (1)$$

For a given plug, the radii r_w (gas-side wall radius), r_a, and r_b are collinear; they are taken perpendicular to the gas-side surface of the nozzle and extend to the centerline; T_a and T_b are internal wall temperatures measured with the thermocouples embedded in the plug. The thermal conductivity k is the arithmetic average of the values at T_a and T_b.

The gas-side wall temperatures determined from the different thermocouple combinations in each plug were generally within 1%. However, in determining the wall heat flux from Eq. (1), there were inconsistencies. If the center thermocouple and the one nearest the gas-side wall were used, the calculated wall heat flux was on the average about 10% higher than with the thermocouple nearest the gas-side and water-side walls. With a combination of the center thermocouple and the one nearest the gas-side wall, the total heat load was found to agree within 5% of that computed from the coolant flow rate and the coolant temperature rise; consequently, these two thermocouples were used to calculate the wall heat flux. The estimated errors resulting from the use of these thermocouples are discussed near the end of the Appendix.

The heat-transfer coefficient was computed by

$$h = \frac{q_w}{T_{aw} - T_w} \qquad (2)$$

The adiabatic wall temperature was calculated by taking the recovery factor equal to 0.89. This value is based on measurements with air accelerated over a flat plate by convergent opposite wall (Ref. 8) and by extrapolating wall temperatures to the zero heat-flux condition for a flow through a nozzle (Ref. 4). In both of these investigations, the recovery factor was found to be independent of pressure gradient. Actually, for the large difference between the stagnation and wall temperatures in the present results, the calculated heat-transfer coefficients are insensitive to the assumed recovery-factor dependence

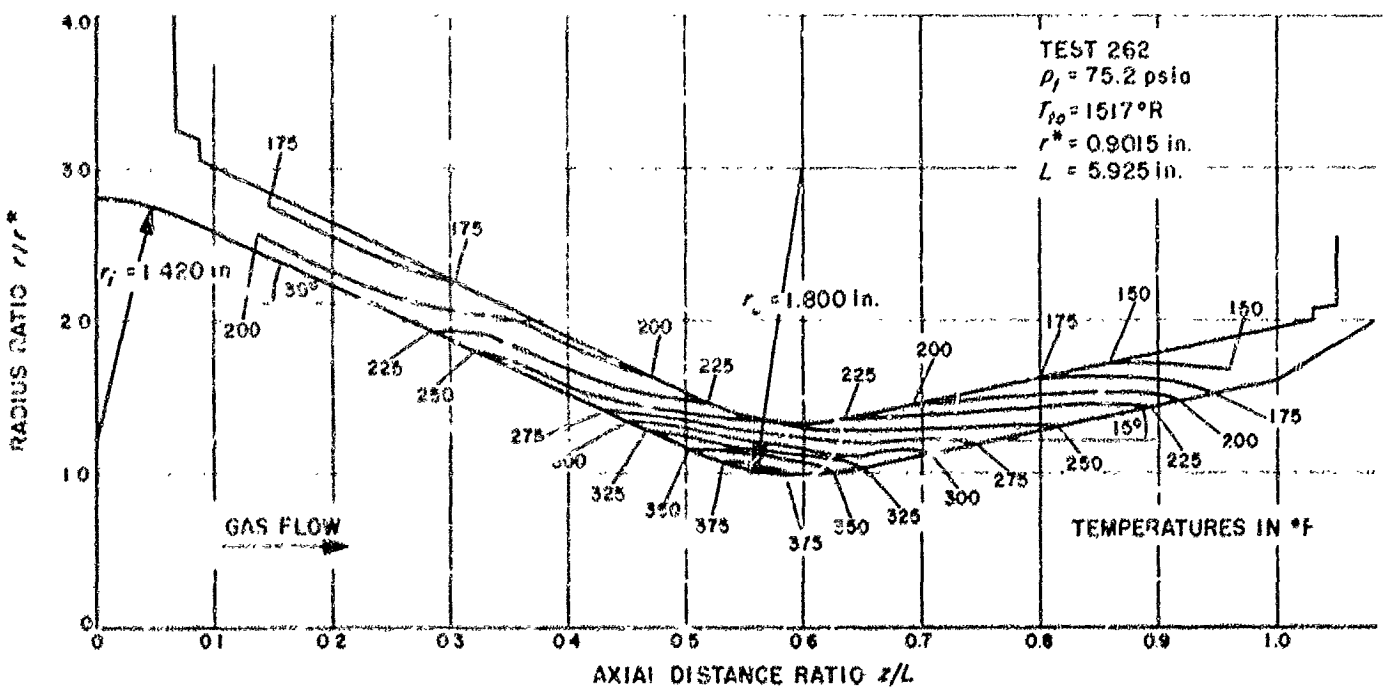

Fig. 5. Nozzle wall isotherms

IV. STATIC PRESSURE AND MASS FLUX DISTRIBUTIONS

The measured static-to-stagnation pressure ratio along the nozzle is shown in Fig. 6 at a stagnation temperature of 1500°R for a range of stagnation pressures from 45 to 150 psia. Measurements at higher stagnation pressures were not possible because of manometer limitation. Except in the nozzle-exit region, where the rapid rise in static pressure at the lower stagnation pressures indicates flow separation, the pressure-ratio distribution is nearly invariant. For computational purposes, it is assumed to be invariant above 150 psia. Deviations of measured pressure distributions from that predicted from one-dimensional isentropic flow are indicated. The deviations result from radial-velocity components caused by the taper and curvature of the nozzle and are as large as 30% just downstream of the throat.

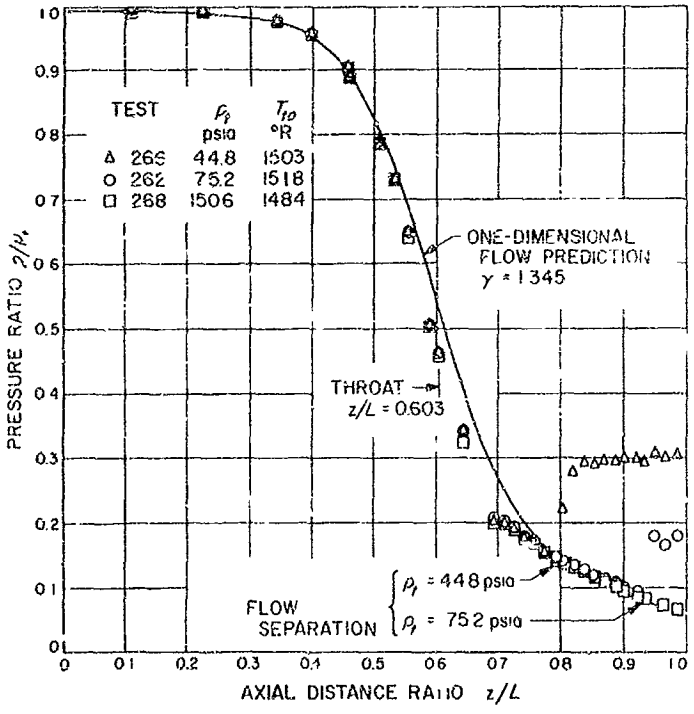

Fig. 6. Ratio of static to stagnation pressure along the nozzle

In Fig. 7, the ratio of the local mass flux $\rho_e u_e$, calculated from the measured wall static pressures, to that predicted from one-dimensional flow $\rho_1 u_1$, is shown at p_i = 75 psia for different stagnation temperatures and cooled approach lengths. For the tests shown, the maximum value of the mass flux $\rho_e u_e$ occurred at z/L = 0.58. This location corresponds to the intersection of the sonic

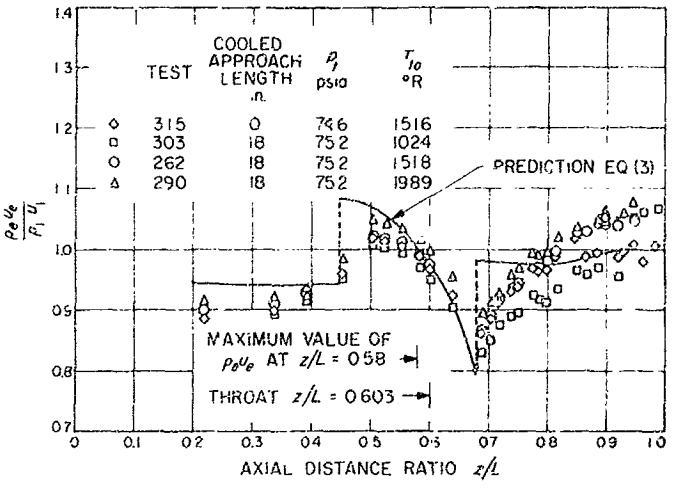

Fig. 7. Ratio of local to one-dimensional mass flux along the nozzle

line with the nozzle wall and is upstream of the geometric throat, which is located at z/L = 0.603. Just downstream of the throat there is a sharp dip in the mass-flux ratio, the reduction below that predicted from one-dimensional flow amounting to about 15%. There appears to be a slight trend toward mass-flux ratios increasing with stagnation temperature, especially near the nozzle exit. The effect of boundary-layer thickness at the nozzle inlet on the mass-flux ratio is negligible.

Since the deviations from one-dimensional flow are significant in the throat region, it is of interest to determine to what extent the mass flux at the edge of the boundary layer is predictable. Oswatitsch and Rothstein (Ref. 9) considered isentropic, two-dimensional flow in a convergent–divergent nozzle. The wall boundary layer is neglected as is the requirement that the fluid velocity at the wall be exactly parallel to it. The final result of their analysis can be cast in the form of a ratio of the mass flux at the nozzle wall to that for one-dimensional flow

$$\frac{\rho_e u_e}{\rho_1 u_1} = \frac{\left\{1 - \frac{\gamma - 1}{2}\left(M_1 \frac{a_1}{a_0}\right)^2 \left(\frac{u_e}{u_1}\right)^2\right\}^{\frac{1}{\gamma-1}}}{\frac{p_1}{p_0}} \frac{u_e}{u_1} \qquad (3)$$

where

$$\frac{u_e}{u_1} = \sqrt{\left\{1 + \frac{1}{2}\left[\frac{1}{2}\, r\, \frac{d^2r}{dz^2} + \frac{1}{4}\, \frac{\frac{du_1}{dz}}{u_1}\, r\, \frac{dr}{dz} - \left(\frac{dr}{dz}\right)^2\right]\right\}^2 + \left(\frac{dr}{dz}\right)^2}$$

The predicted mass-flux ratio is only a function of the nozzle configuration, with the subscript 1 denoting average quantities for one-dimensional flow. The prediction shown in Fig. 7 is in fair agreement with the data in the throat region. It also indicates the sonic line to be upstream of the throat. At the intersection of the conical sections of the nozzle with the throat curvature, there is a predicted discontinuity in the mass-flux ratio as indicated by the dashed lines. The prediction is not shown in the nozzle-entrance region, since there, restrictions on the magnitude of the nozzle radius and its derivatives implied in the analysis are not satisfied. Even in the throat region, these are marginal.

V. BOUNDARY LAYERS AT THE NOZZLE INLET

To indicate the nature of the boundary layer at the nozzle inlet with the 18-in. cooled approach length, the velocity ratio u/u_e, mass-flux ratio $\rho u/\rho_e u_e$, and stagnation-temperature distribution $(T_t - T_w)/(T_{te} - T_w)$ are shown in Fig. 8 for a stagnation temperature of 1500°R and a range of stagnation pressures from 45 to 254 psia. The profiles indicate that the boundary layers are turbulent over the range of stagnation pressures. A 1/7-power-law curve for negligible property variation across the boundary layer is shown for comparison. Values of the thicknesses δ^*, θ, and ϕ near the nozzle inlet were calculated by taking into account the mass, momentum, and energy defects for flow through a pipe of radius R.

$$\delta^*\left(R - \frac{\delta^*}{2}\right) = \int_0^r \left(1 - \frac{\rho u}{\rho_e u_e}\right)(R - y)\, dy \quad (4)$$

$$\theta\left(R - \frac{\theta}{2}\right) = \int_0^r \frac{\rho u}{\rho_e u_e}\left(1 - \frac{u}{u_e}\right)(R - y)\, dy \quad (5$$

$$\phi\left(R - \frac{\phi}{2}\right) = \int_0^r \frac{\rho u}{\rho_e u_e}\left[1 - \left(\frac{T_t - T_w}{T_{te} - T_w}\right)\right](R - y)\, dy \quad (.$$

In general, these thicknesses are about 5% lower tha those obtained by assuming flow over a plane surfac The effect of increasing stagnation pressures is to decrea the displacement, momentum, and energy thicknesses.

In Fig. 9, the velocity profiles of Fig. 8 are shown i terms of $u^+ = u/(\sqrt{\tau_w/\rho_e})$ and $y^+ = (y\sqrt{\tau_w/\rho_e})/\nu_e$. Th wall shear was determined by matching the profiles i

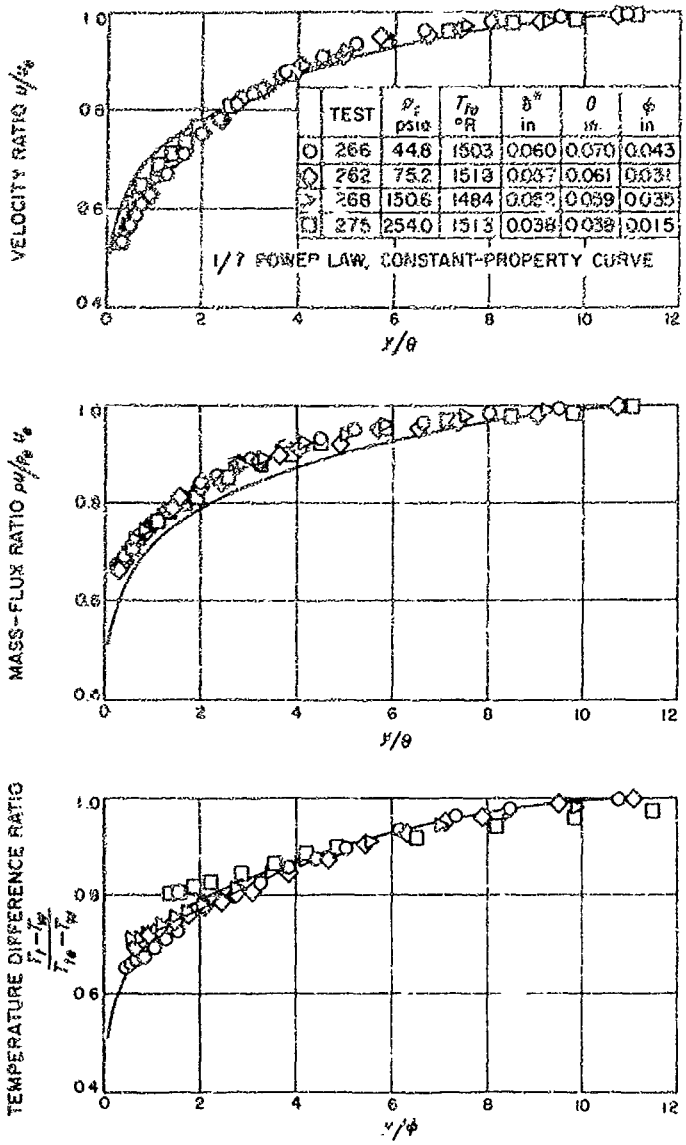

Fig. 8. Boundary-layer profiles 1.25 in. upstream of nozzle inlet with 18-in. cooled approach length

the wall vicinity to the "law of the wall," which was taken in the form

$$u^+ = 5.5 + 2.5 \ln y^+ \qquad \text{for } y^+ > 30 \tag{7}$$

In the wall vicinity, the "law of the wall" appears to be valid, and in the outer part of the boundary layer, the departure is typical of the "law of the wake" proposed by Coles (Ref. 10). Shown in two ways in Fig. 9 are the friction coefficients, $c_f/2 = \tau_w/(\rho_e u_e^2)$, predicted from the Blasius flat-plate relation

$$\frac{\tau_w}{\rho u_e^2} = \frac{0.0128}{\left(\dfrac{\rho u_e \theta}{\mu}\right)^{1/4}} \tag{8}$$

With properties ρ and μ evaluated at the free-stream temperature, the predictions exceed those deduced from matching to the "law of the wall" by about 20%. With properties evaluated at the film temperature, the predictions are about 55% higher. Also shown in the Figure are the friction coefficients predicted from the boundary layer analysis of Ref. 11, which is discussed in Section VII. These predictions are nearer those deduced from the "law of the wall," though they are still high.

At the other stagnation temperatures of 1030 and 2000°R, as well as with the shorter cooled approach lengths of 6 and 12 in., the boundary-layer profiles (not shown) were also turbulent. However, with no cooled approach length, the boundary layer appears to be in the transition region, as indicated by the velocity profiles shown in Fig. 10. These profiles lie between a turbulent and laminar one, as shown by the 1/7-power law and Blasius' laminar-flow profiles.

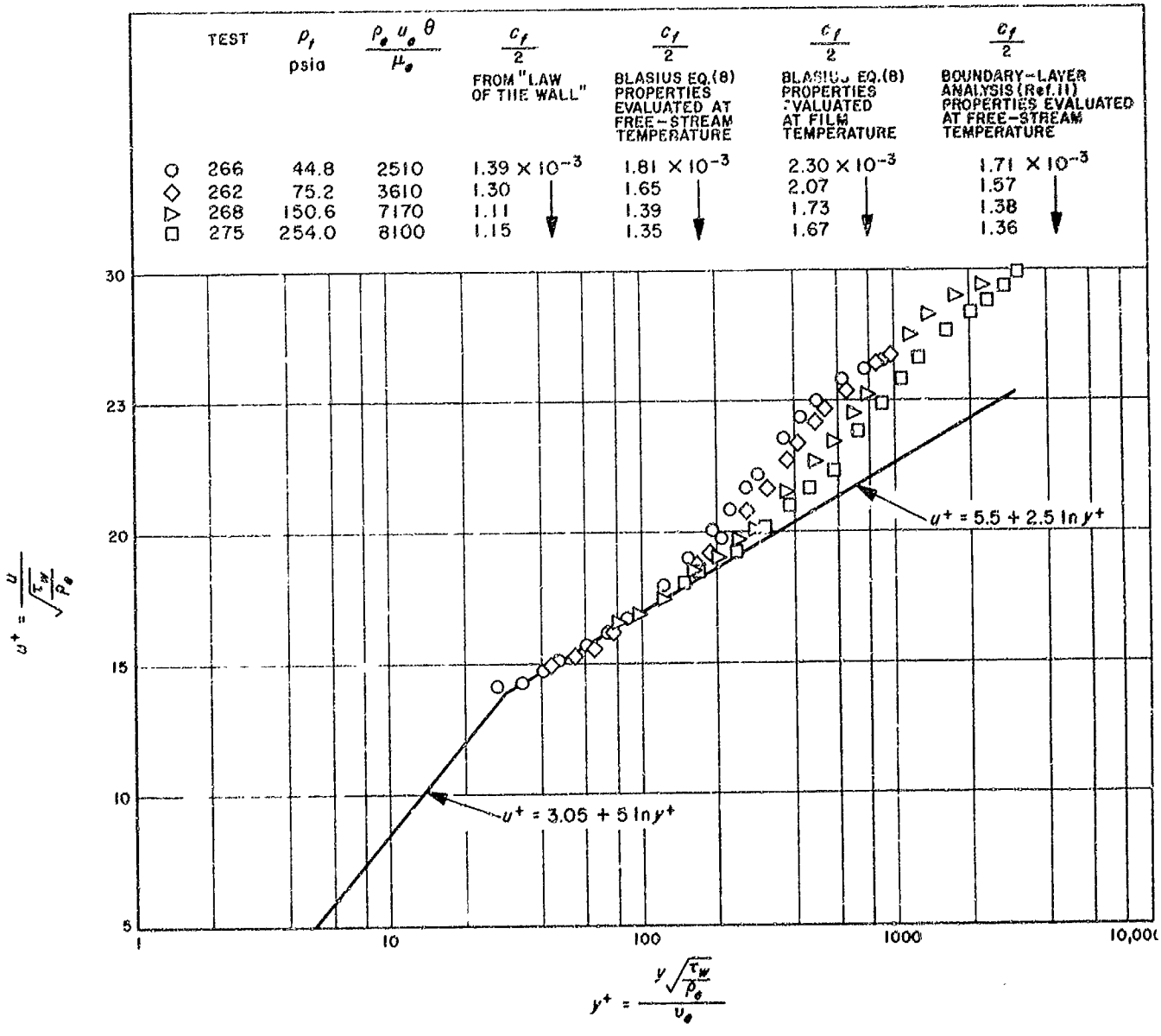

Fig. 9. Velocity distributions 1.25 in. upstream of nozzle inlet with 18-in. cooled approach length

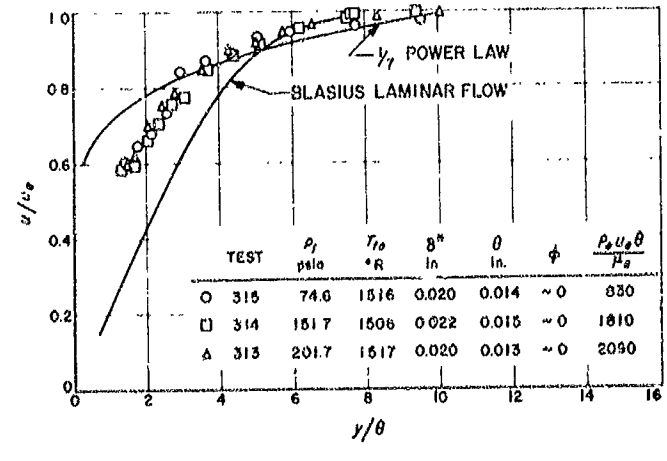

Fig. 10. Velocity profiles 1.25 in. upstream of nozzl inlet without cooled approach length

VI. HEAT-TRANSFER RESULTS

The variation of the heat-transfer coefficient along the nozzle with the 18-in. cooled approach length is shown in Fig. 11 for stagnation temperatures of about 1030, 1500, and 2000°R and a range of stagnation pressures from 30 to 254 psia. At the highest stagnation temperature, it was not possible to obtain data above a stagnation pressure of 125 psia because of temperature limitations on the wall-thermocouple insulating material. The curves in the Figure were faired through the data. It is evident that during a given test, circumferential variations in heat transfer did exist, as indicated by the symbols which are tagged alike. These indicate thermocouple plugs spaced within 55 deg of each other. A certain amount of consistency can be deduced by comparing data obtained from the same thermocouple plugs for different tests. The majority of the tests were duplicated and found reproducible to within ±2%. It was not possible to explain these variations by nonuniformities in the flow based on measurements in the gas stream at the nozzle inlet. However, it is possible that nonuniformities could have existed in the boundary layer.

The heat-transfer coefficients in Fig. 11 increase, as expected, with increasing stagnation pressures as a result of larger mass fluxes; however, their variation with stagnation temperature at the different stagnation pressures is less clear, with the trends dependent on stagnation pressure. The maximum value of the heat-transfer coefficients occurs just upstream of the throat in the vicinity where the mass flux $\rho_e u_e$, as indicated in Fig. 7, is a maximum. A substantial decrease in heat transfer downstream of the point of flow separation which occurred at the low stagnation pressures is indicated by the tests at a stagnation pressure of 45 psia. At the lowest stagnation pressure, the data are not shown in this region, since there were large fluctuations in the wall-thermocouple readings.

To represent the heat-transfer results shown in Fig. 11 in terms of correlation parameters commonly used involves both the selection of a characteristic length and the temperature at which properties are evaluated. In Fig. 12 there are shown, in addition to the data of Fig. 11, data from many more tests at intermediate stagnation pressures presented in terms of the group, $St\ Pr^{0.6}$, and the Reynolds number based on the nozzle local diameter. Fluid properties were evaluated at the static temperature at the edge of the boundary layer, and the mass flux $\rho_e u_e$ was used to compute both the Stanton and Reynolds numbers. The variation of viscosity, specific heat, and Prandtl number with temperature for air was obtained from Ref. 12. Each of the plots in Fig. 12 indicates the heat-transfer data obtained at a single area ratio or axial station. Hence, in each of the plots, increasing Reynolds numbers ($\rho_e u_e D/\mu_e$) at the different stagnation temperatures correspond directly to increasing stagnation pressures, since the nozzle diameter is constant.

Proceeding through the subsonic part of the nozzle (decreasing area ratios), there is a substantial reduction in heat transfer at the lower stagnation pressures below that typical of a turbulent boundary layer (Curve A) where the dependence of the heat-transfer coefficient on the mass flux is $h\alpha(\rho_e u_e)^{4/5}$. This reduction persists through the throat and into the supersonic region. It could actually continue to the exit of the nozzle; however, in these tests it was not possible to operate the nozzle without separation near the exit at low stagnation pressures. Measurements in separated regions are not shown. At the higher stagnation pressures (higher Reynolds numbers), above 75 psia, the heat transfer is typical of a turbulent boundary layer.

Other investigators have observed unexpected trends accompanying the acceleration of turbulent boundary layers. The trends shown in Fig. 12 are similar to the results of Ref. 1, which were obtained from rocket-engine tests over a similar range of stagnation pressures. The large positive slope of the experimental curves at area ratios near 1 was noted as well as the eventual decrease in slope with increasing stagnation pressure. This implies that for the rocket-engine tests, injection and combustion effects did not substantially alter the heat-transfer trends from those indicated in Fig. 12. In Ref. 13, a turbulent boundary layer at the entrance of a supersonic nozzle was found to undergo transition to a nearly laminar one at the nozzle exit. The stagnation pressure was 4.3 psia. When the stagnation pressure was increased to 14.2 psia, a turbulent boundary layer was found at the nozzle exit. No boundary-layer measurements were made within the nozzle. In Ref. 14, it was observed that heat-transfer trends of the type seen here at the low stagnation pressures existed under lower pressure-gradient conditions. There was departure from fully turbulent flow through the acceleration region as indicated by the linearity of the measured velocity profiles in the wall vicinity.

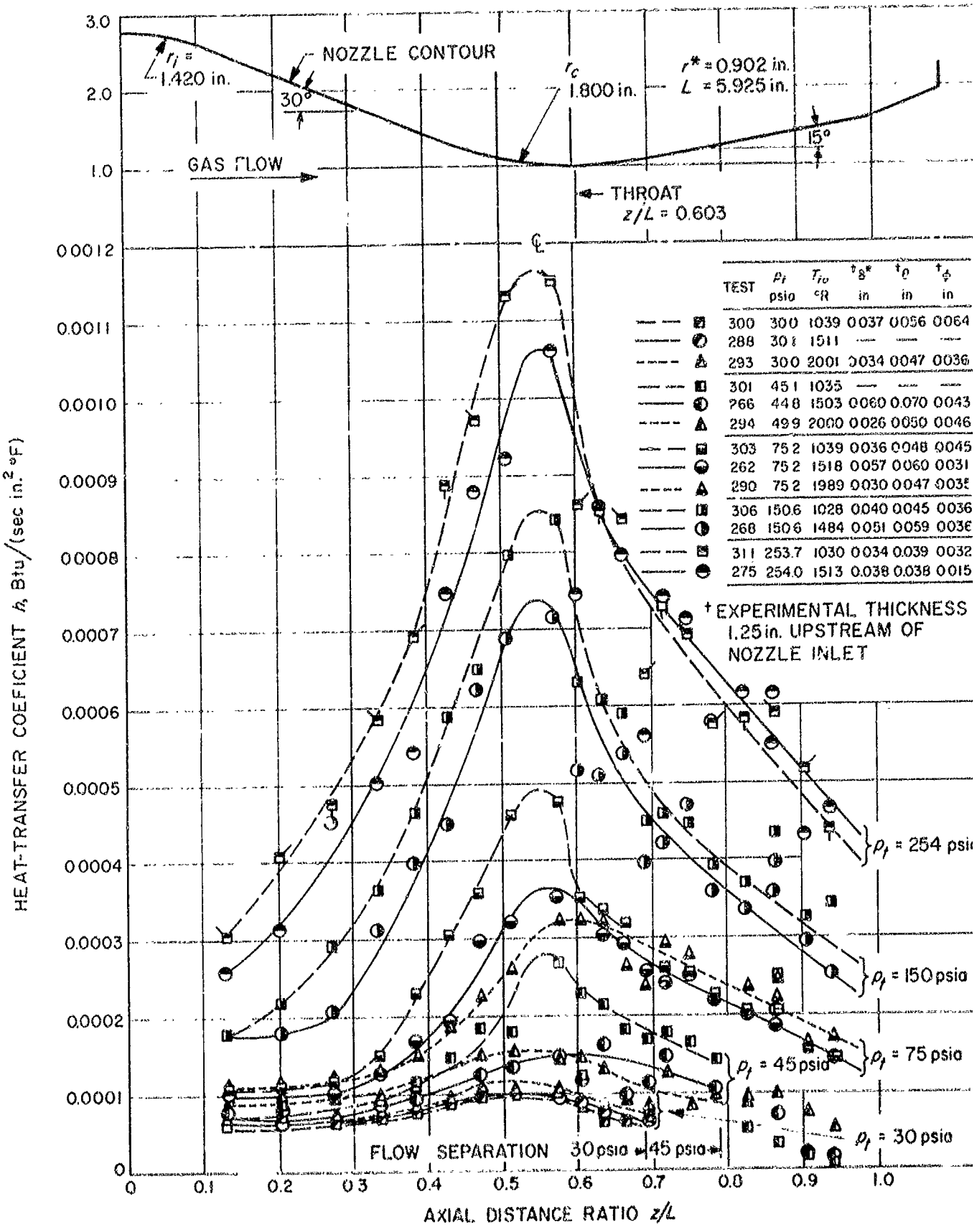

Fig. 11. Heat-transfer coefficient vs. axial distance ratio with 18-in. cooled approach length

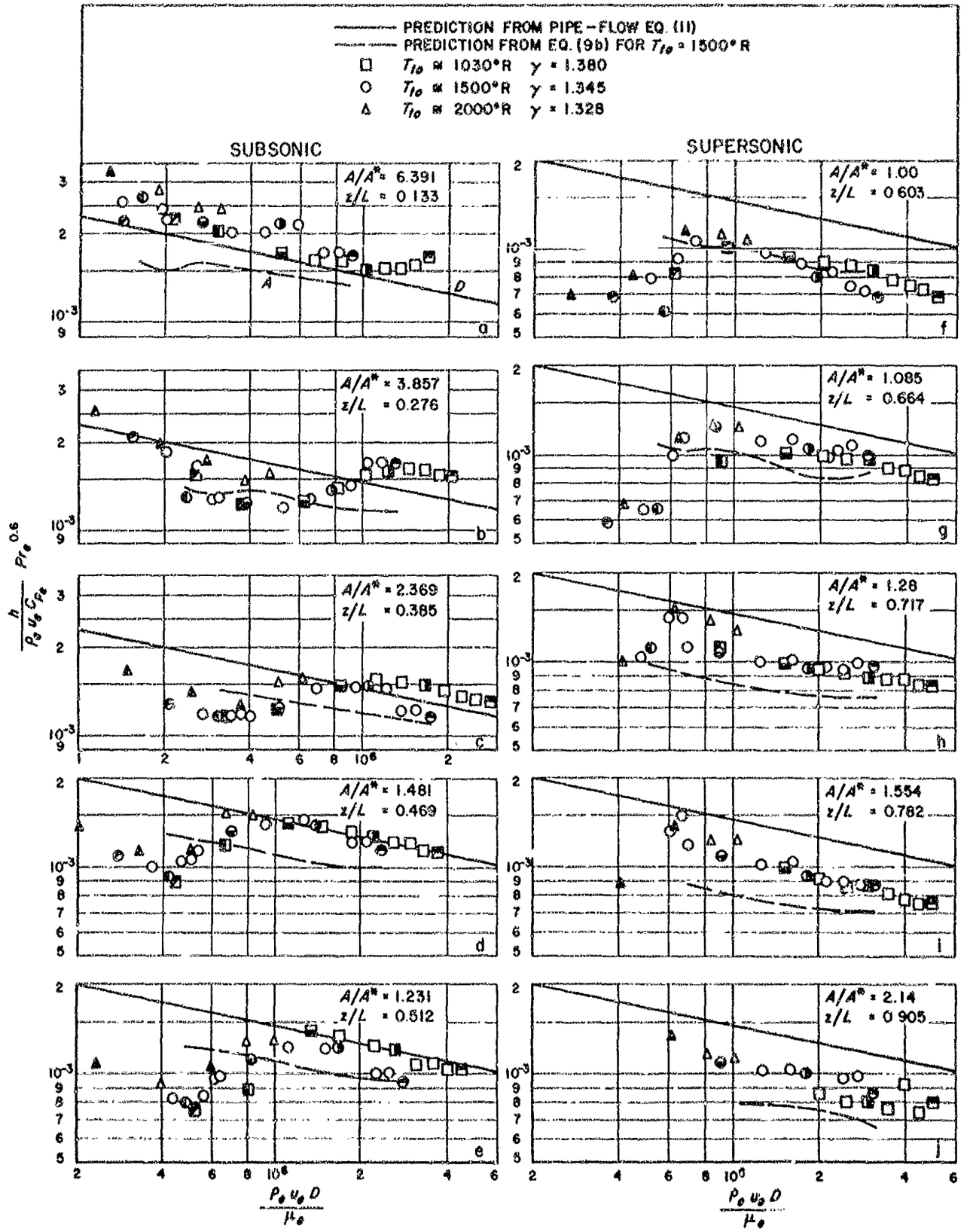

Fig. 12. Heat-transfer results at various subsonic and supersonic area ratios with 18-in. cooled approach length

From these observations, it seems logical to speculate hat at the lower stagnation pressures, the boundary ayer may have undergone transition from the turbulent profile at the nozzle inlet to a partially laminar profile nder the influence of the large, favorable pressure gradient. The consequent decrease in eddy transport would reduce both the wall friction and heat transfer. n Section VIII, a parameter relating a predicted reduction in net production of turbulent kinetic energy to the ow stagnation pressures is discussed.

To indicate the variation of the Stanton number with Reynolds number along the nozzle, a few of the tests om Fig. 11 are shown again in Fig. 13. To help identify he axial location in terms of the Reynolds number, the neasuring station nearest the nozzle inlet is noted and the data points in the supersonic region are tagged. No additional information is shown in this Figure; however, the trends of conditions along the nozzle are more evident than in Fig. 11. Again, the data downstream of the nozzle-inlet region for the lowest stagnation pressure deviate furthest from the $(\rho_e u_e)^{4/5}$ dependency, which is shown as a reference curve.

The effect of varying nozzle-inlet boundary-layer thicknesses on the heat transfer is shown in Fig. 14, in particular for a stagnation temperature of 1500°R and a range of stagnation pressures from 75 to 200 psia. With no cooled approach length, for which the ratio of estimated boundary-layer thickness to nozzle-inlet radius is about 0.05, the heat-transfer coefficient is above the thicker layer results. This trend persists through the nozzle and

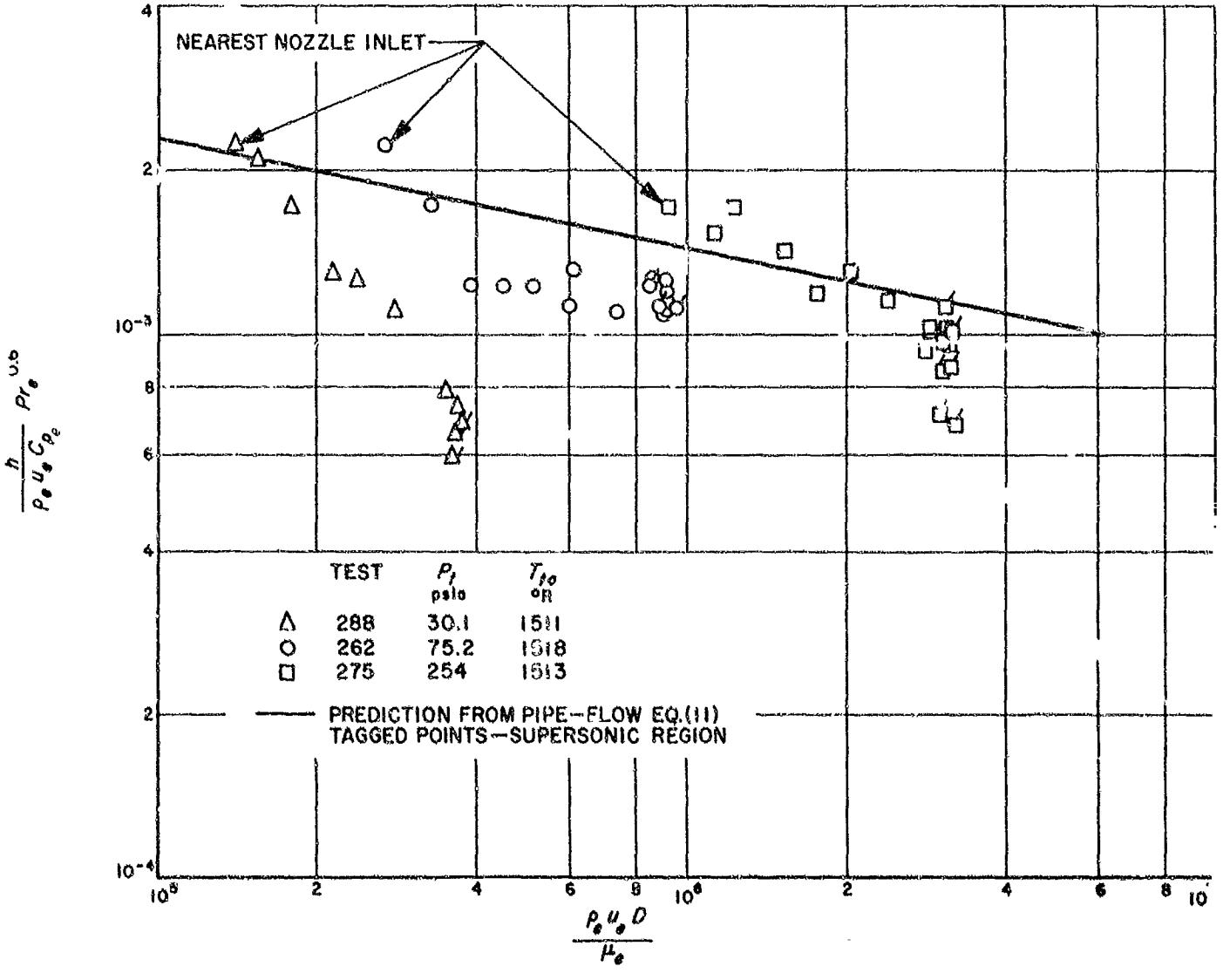

Fig. 13. Heat-transfer results along nozzle with 18-in. cooled approach length

extends into the supersonic region. Just upstream of the throat, where the heat-transfer coefficient is a maximum, the thinnest layer results exceed the thickest layer results obtained with the 18-in. cooled approach length by about 10%. Apparently, with no cooled approach length, transition from the boundary-layer profile shown in Fig. 10 to a turbulent one occurred upstream of the first heat-transfer measuring station.

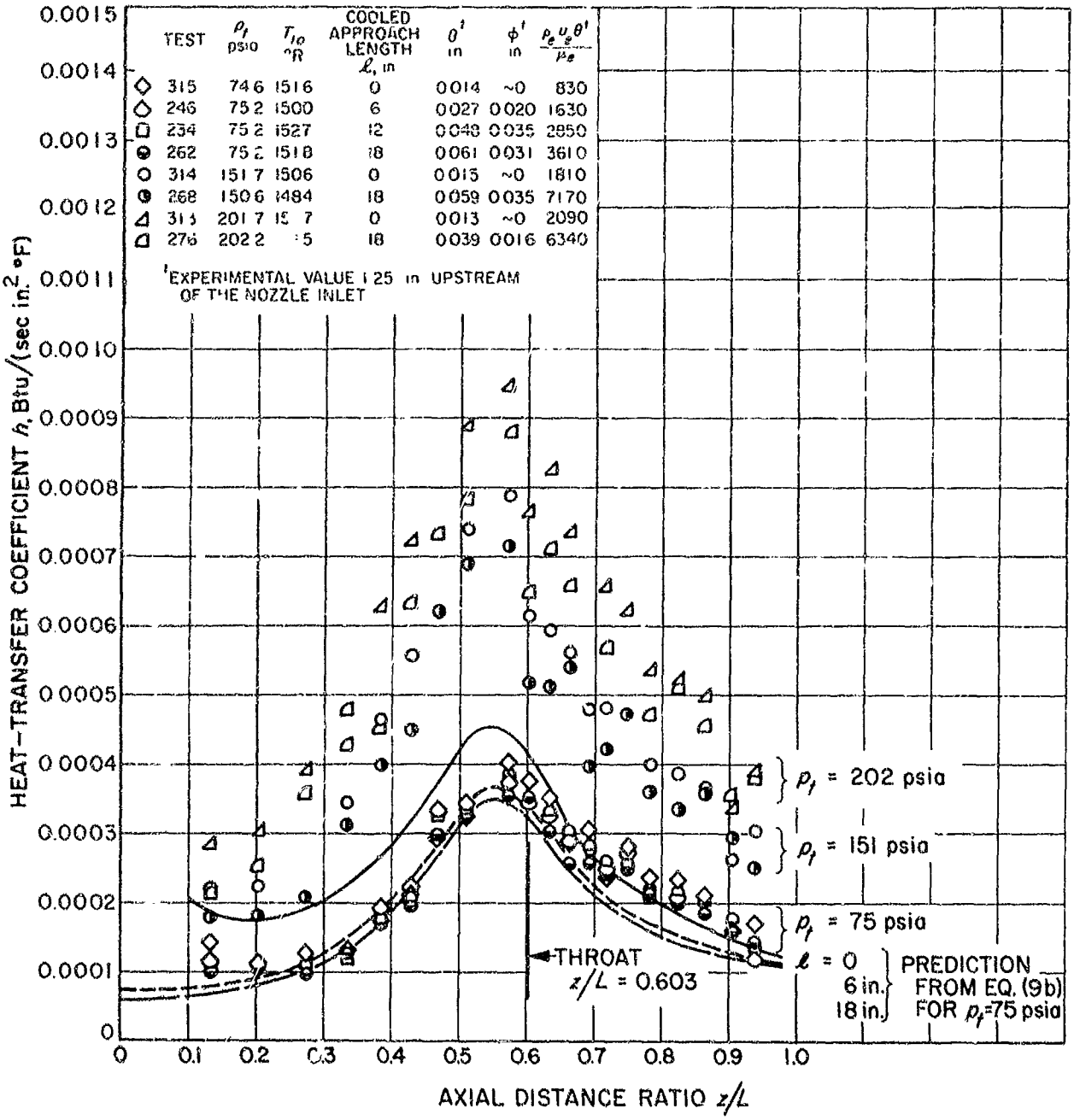

Fig. 14. Heat-transfer coefficients for various boundary-layer thicknesses at nozzle inlet vs. axial distance ratio

VII. COMPARISON OF HEAT-TRANSFER RESULTS WITH PREDICTIONS

Methods of predicting nozzle heat transfer consist either of boundary-layer analyses or, because of their simplicity, of those related to pipe flow. In the boundary-layer analyses (e.g., Refs. 15, 16), the integral forms of the momentum and energy equations are solved based on a number of assumptions, the most important of which is an assumed form of Reynolds analogy between heat transfer and wall friction. A limited amount of data (Refs. 14, 17, 18) for heat transfer to an accelerated, essentially incompressible, turbulent boundary layer where property variations were small has indicated that heat-transfer coefficients determined from the wall friction through one of the analogies known to apply for constant free-stream velocity were far in excess of actual values. However, since boundary-layer measurements were not made in the nozzle, an experimental check was not possible.

Another, more recent, boundary-layer prediction method in which various heat-transfer assumptions can be compared to experimental results is a modification of the turbulent boundary-layer analysis of Ref. 15. In the modified analysis, as in Ref. 15, the integral forms of the momentum and energy equations are solved simultaneously for θ and ϕ. The assumptions involve the specification of the heat-transfer and wall-friction coefficients, and the similarity of the boundary-layer velocity and stagnation-temperature profiles on a 1/7-power-law basis with respect to their individual thicknesses, which can be different from one another. The prediction yields both the flow and thermal characteristics when the nozzle configuration, wall temperature, and free-stream properties are specified. To initiate the prediction, a knowledge of θ and the ratio of thicknesses δ_t/δ is required at one location which was taken at the boundary-layer measuring station 1.25 in. upstream of the nozzle inlet. A complete report on the computation procedure of the modified boundary-layer analysis, which is programmed for numerical solution on an IBM 7090 computer, is presented in Ref. 11.

The heat-transfer specification from the modified turbulent boundary-layer analysis (Ref. 11) is

$$\frac{h}{\rho_e u_e c_p} = K^* \frac{c_f^*}{2} \left(\frac{\phi}{\theta}\right)^n \qquad (9a)$$

where

$$K^* = \left\{\sqrt{\frac{c_f^*}{2}}\left[5\,Pr + 5\ln(5\,Pr + 1) - 14 + \sqrt{\frac{2}{c_f^*}}\right]\right\}$$

The factor K^* is similar to the Prandtl-number correction factor in the von Kármán analogy. The coefficient c_f^* is analogous to the wall friction coefficient but with the momentum thickness dependence replaced by the energy thickness. The ratio $(\phi/\theta)^n$ is a factor included in the analysis. For the present results, stagnation pressures above 75 psia, n was found to have a value near zero. The wall friction coefficient is predicted either from the Blasius flat-plate relation (Eq. 3) with properties ρ and μ evaluated at the film temperature, as was done in the earlier analysis (Ref. 15), or taking the adiabatic wall friction coefficient (predicted from Cole's relation [Ref. 19] between the friction coefficient for a compressible and incompressible flow with properties evaluated at the free-stream temperature. This latter method is suggested by a limited amount of data (Ref. 20), which indicate both the Stanton number and wall friction coefficient with properties evaluated at the free-stream temperature to be insensitive to severe wall cooling. Of note is that for a severely cooled wall the friction coefficient predicted by the latter method is substantially below that predicted by evaluating properties at the film temperature.

Prediction of the heat-transfer coefficient from Eq. (9a) requires both the selection of n and the temperature at which properties are to be evaluated. With $n \simeq 0.1$, the prediction is approximately the same as that of Ref. 15. For comparison purposes, two limiting values of n are considered. These correspond to assuming a Stanton number dependence only on the thermal characteristic ϕ; i.e., $n = 0$, for which Eq. (9a) becomes

$$\frac{h}{\rho_e u_e c_p} = K^* \frac{c_f^*}{2} \qquad (9b)$$

or to taking $n = 0.25$, for which Eq. (9a) becomes approximately the von Kármán analogy

$$\frac{h}{\rho_e u_e c_p} = K \frac{c_f}{2} \qquad (9c)$$

where

$$K = \left\{\sqrt{\frac{c_f}{2}}\left[\,5\,Pr + 5\ln(5\,Pr + 1) - 14 + \sqrt{\frac{2}{c_f}}\right]\right\}^{-1}$$

Other analyses which assume a Stanton-number dependence on ϕ have been made in Refs. 17 and 21 and compared to experimental heat-transfer results for accelerated turbulent boundary-layer flows. In Ref. 17, the predictions exceeded the data by about 30% in part of the acceleration region, while in Ref. 21, the correspondence with the data was good.

The heat-transfer predictions shown in Fig. 15 as curve A are from Eq. (9b) for a stagnation temperature of 1500°R and a range of stagnation pressures from 45 to 254 psia, with the 18-in. cooled approach length. These predictions were made with properties evaluated at the free-stream temperature and conditions at the edge of the boundary layer determined from the wall static-pressure measurements. Shown as curve C in Fig. 15 is the prediction from Eq. (10), in which the friction coefficient $c_f/2$ was determined from the modified turbulent boundary-layer analysis. The reduction in the predicted heat-transfer coefficients provided by Eq. (9b) below the von Kármán analogy is due to the greater predicted thermal than velocity boundary-layer thicknesses through the nozzle. At the highest stagnation pressure, the predicted ratios of ϕ/θ as indicated in Fig. 16 are as large as 6 in the throat region. At the 75-psia stagnation pressure, the correspondence of the prediction from the modified turbulent boundary-layer analysis, Eq. (9b), with the data is good except near the nozzle exit. At the highest stagnation pressure of 254 psia, where the circumferential variation of the data is considerable, the correspondence with the averaged heat-transfer data is fair. The reproducibility of the data in Fig. 15 for 254 psia is indicated by the two sets of data shown by the open and shaded symbols. At the lowest stagnation pressure, p_t = 44.8 psia, the prediction exceeds the data by as much as 50% in the throat region. For the range of stagnation pressures, the predicted maximum value of the heat-transfer coefficient is just upstream of the throat, in agreement with the data.

The effect of temperature choice for property evaluation may be observed in Fig. 15 by comparing curves A and B. Curve B represents Eq. (9b) with properties evaluated at the film temperature T_f. In the throat region, it lies above the data but is in better agreement near the nozzle exit than curve A.

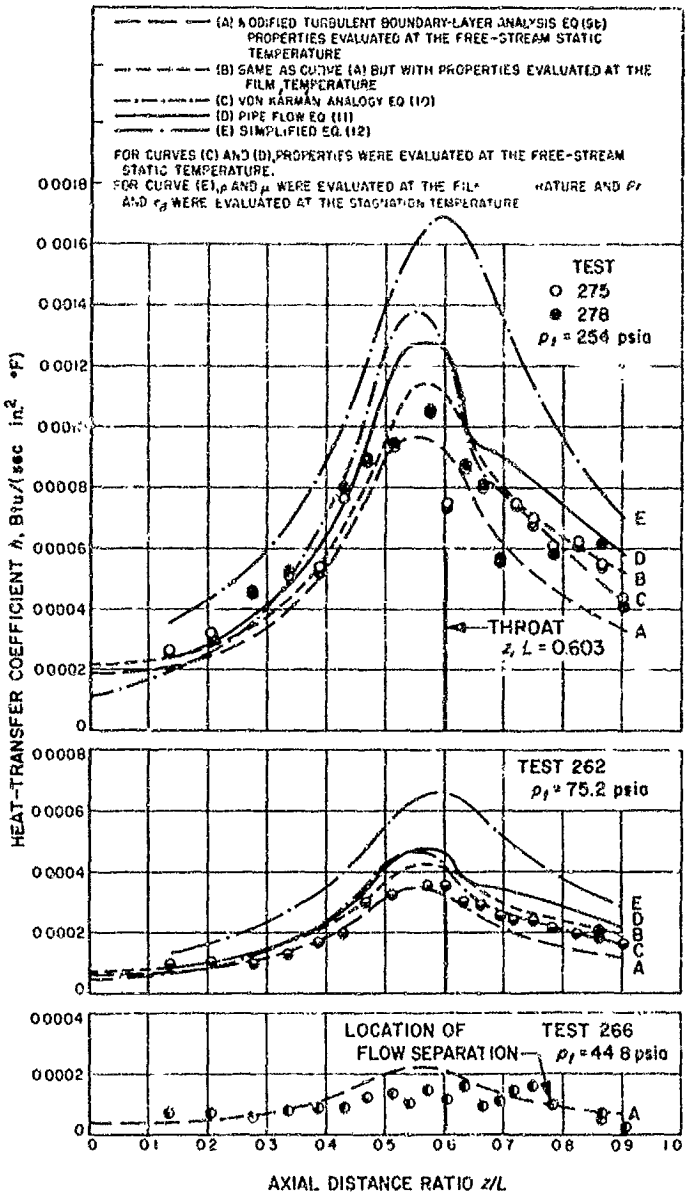

Fig. 15. Comparison of experimental heat-transfer coefficients with predictions at T_{t_0} = 1500°R with 18-in. cooled approach length

For comparison, the predictions from the following form of the pipe-flow equation for fully developed flow in which both the thermal and velocity boundary layer extend to the centerline and there is no significant pressure gradient are shown as curve D in Fig. 15.

$$St\,Pr^{0.6} = 0.023\,Re_h^{-0.2} \qquad (11)$$

Also shown, as curve E in Fig. 15, is the equation of Ref. 22:

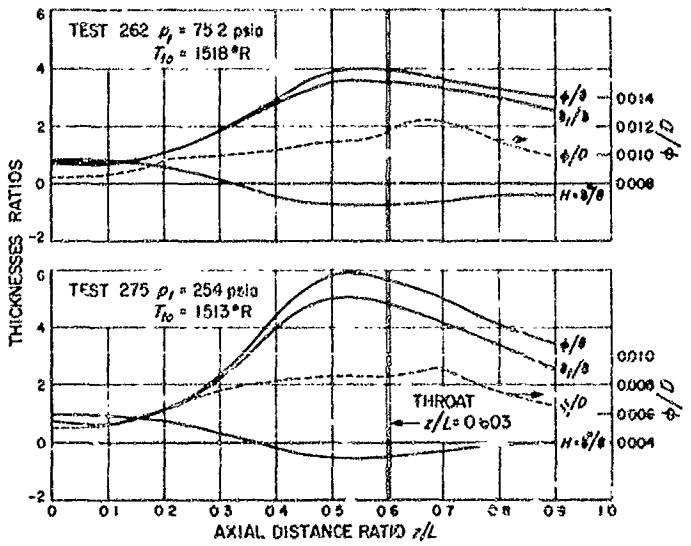

Fig. 16. Predicted thickness ratios along nozzle with 18-in. cooled approach length

$$h = \left[\frac{0.026}{(D^*)^{0.2}}\left(\frac{\mu^{0.2}c_p}{Pr^{0.6}}\right)_0\left(\frac{p_0 g_c}{c^*}\right)^{0.8}\left(\frac{D^*}{r_c}\right)^{0.1}\right]\left(\frac{A^*}{A}\right)^{0.9}\sigma \tag{12}$$

In the pipe-flow equation, all properties were evaluated at the free-stream static temperature, while in Eq. (12), the Prandtl number and specific heat were assumed constant at their stagnation temperature values and ρ and μ were evaluated at the film temperature. In Eq. (12), one-dimensional flow quantities were used, since two-dimensional effects are not taken into account in the derivation. If they were, the prediction would be nearer that of the pipe-flow equation. Two-dimensional values of local mass flux are 15% below the one-dimensional values just downstream of the nozzle throat, as seen in Fig. 7. The prediction from Eq. (12) exceeds the data by as much as 80% in the throat region. The pipe-flow prediction, Eq. (11), though in better agreement with the data, is still about 25% high at the throat.

From these observations, it appears that fair agreement with the data is provided at the higher stagnation pressures by the modified boundary-layer analysis taken in the form of Eq. (9b), with properties evaluated at the free-stream static temperature. These predictions are also shown, along with others, at the intermediate pressures of p_t = 50 and 150 psia for T_{to} = 1500°R, as curve A in Fig. 12. The predicted Stanton-number dependence on the mass flux is approximately that of the pipe-flow equation, which is shown as curve D. However, the prediction for all the axial locations cannot be approximated by a equation like the pipe-flow equation but with a lower coefficient because of the variation of the predicted value of ϕ relative to D. For a given run, ϕ decreases through the subsonic region, attaining a minimum near the throat and then increases in the supersonic region, qualitatively similar but not in direct correspondence with the nozzle diameter. A few of these predicted ratios are shown in Fig. 16.

In Figs. 12c through 12i, the reduction in heat transfer at Reynolds numbers, Re_{x_0}, less than about 8×10^5 not predictable from an analysis for a turbulent boundary layer, as indicated by the prediction from Eq. (9b) shown in Fig. 12 as curve A.

Predictions from Eq. (9b) (not shown) were also made at stagnation temperatures of 1030 and 2000°R, with 18-in. cooled approach length. The magnitude of the decrease in the heat-transfer coefficient with increasing stagnation temperature at the higher stagnation pressure shown in Fig. 11 was not predictable. From Eq. (9b), the dependence of the heat-transfer coefficient on stagnation temperature at a given stagnation pressure is near $h \propto T_{to}^{-0.28}\,\phi^{-0.2}$. However, the energy thickness at the nozzle inlet decreased with increasing stagnation temperature, such that the difference in predicted heat-transfer coefficients was substantially less than exhibited by the data.

The trend of higher heat-transfer coefficients through the nozzle with thinner boundary layers at the nozzle inlet is shown in Fig. 14 to be predictable from Eq. (9). However, the magnitude of the predicted increase should probably be estimated from the 6- and 18-in. cooled approach length predictions. For the zero cooled approach length prediction, wall cooling was assumed to begin at the nozzle inlet. To require that the Stanton number remain finite there, the energy thickness was taken as a small value equal to 0.001 in.

VIII. SOME ADDITIONAL OBSERVATIONS OF THE FLOW AND THERMAL CHARACTERISTICS

In this Section, some features of the flow are shown which depend on the predicted flow and thermal characteristics obtained from the modified turbulent boundary-layer analysis (Ref. 11), with properties evaluated at the free-stream temperature. In Fig. 16, the predicted ratios of ϕ/θ and δ_{t}/δ indicate the thicker predicted thermal than velocity boundary layers, especially in the throat region. Because of the cooled wall, the displacement thickness δ^* becomes negative upstream of the throat, as does $H = \delta^*/\theta$.

In Fig. 17, the predicted momentum thickness Reynolds numbers are a minimum a considerable distance upstream of the throat. At the lowest stagnation pressure, where the heat transfer is below that typical of a turbulent boundary layer, the minimum Reynolds number is 1500. Although this predicted value is probably different from the actual value, it is still considerably above the measured value of 600 found in Ref. 14, below which there was departure from fully turbulent flow. For the case of constant free-stream velocity, Preston (Ref. 23) proposed a value of 320 above which the flow could be considered fully turbulent; for accelerated flows he estimated that the limit might be lower.

To indicate the magnitude of the forces acting on the boundary layer through the nozzle, the ratio of the pressure forces which tend to accelerate the boundary-layer flow to the retardation wall shear forces is shown in Fig. 18 as

$$-\frac{\delta \dfrac{dp}{dx}}{\tau_w}$$

In this ratio the pressure gradient was numerically approximated from the wall static pressure measurements downstream of $x/L = 0.2$. In the nozzle inlet section where the pressure gradient was difficult to obtain numerically, one-dimensional flow was assumed which provided an analytical relation for the pressure gradient. The ratio is largest in the convergent section before decreasing through the throat and divergent section. For comparison, the value of the ratio for fully developed flow in a circular pipe is shown to demonstrate the large flow accelerations in a nozzle.

To gain some knowledge of the mechanism which at the low stagnation pressures reduces the heat transfer

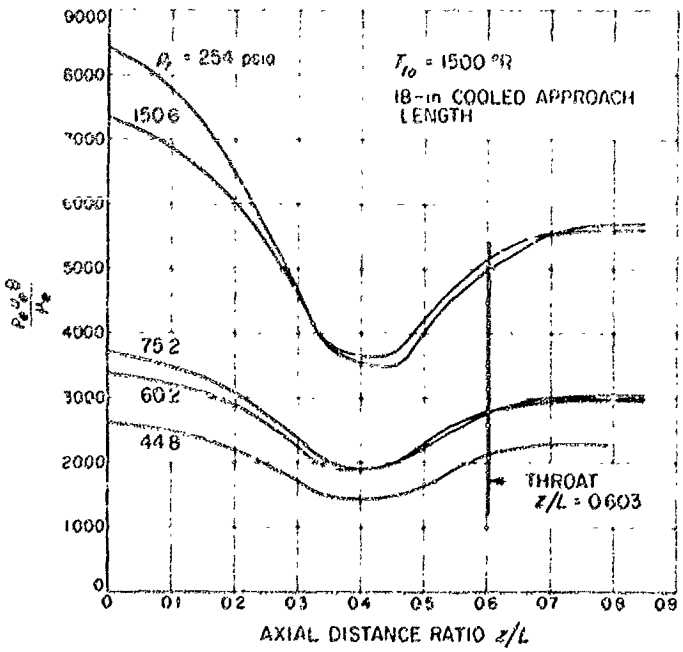

Fig. 17. Predicted momentum thickness Reynolds numbers along nozzle

below that typical of a fully turbulent boundary layer, reference is made to the boundary-layer turbulence energy equation (e.g., Ref. 24). For simplicity, an incompressible plane flow is assumed for which the convection of turbulent kinetic energy by the mean flow is

$$u_j \frac{\partial \overline{\frac{q^2}{2}}}{\partial x_j} = -\overline{u_i' u_j'} \frac{\partial u_i}{\partial x_j}$$

(a)

$$-\frac{\partial}{\partial x_j}\overline{u_j'\left(\frac{p'}{\rho}+\frac{q^2}{2}\right)} + \nu \overline{u_i' \frac{\partial^2 u_i'}{\partial x_j^2}} \qquad (13)$$

(b) (c) (d)

The terms represent the following:

(a) Production of turbulent kinetic energy by the working of the mean velocity gradients against the Reynolds stresses.

(b) Work done by the turbulence against the fluctuation pressure gradients.

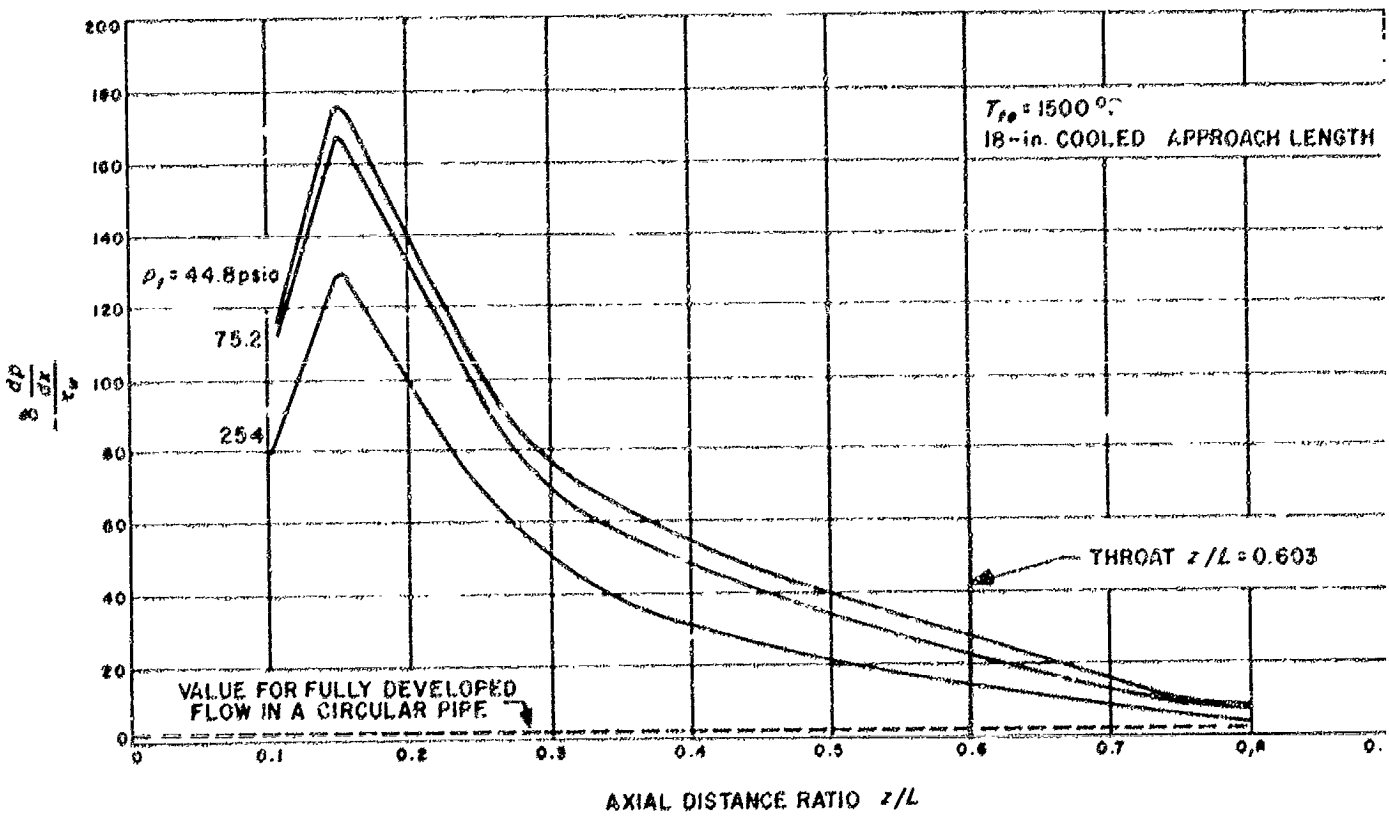

Fig. 18. Predicted ratio of pressure to wall shear forces acting on boundary layer along nozzle

(c) Convection of turbulent kinetic energy by the turbulence itself.

(d) Transfer of energy by the working of the turbulent viscous stresses.

For a two-dimensional flow with a pressure gradient, the significant terms from term (a) that lead to a production or decay of convected turbulent kinetic energy are

$$-\overline{u_i' u_j'} \frac{\partial u_i}{\partial x_j} = -\overline{u'v'} \frac{\partial u}{\partial y} - (\overline{u^2} - \overline{v^2}) \frac{\partial u}{\partial x} \qquad (14)$$

The remaining terms (b), (c), and (d) in Eq. (13) are dependent on the turbulence produced. The first term in Eq. (14) is always positive and leads to a production of turbulent kinetic energy. However, with flow acceleration $\partial u/\partial x > 0$, the second term leads to a decay of turbulent kinetic energy provided that $\overline{u^2} > \overline{v^2}$. Thus, a measure of the importance of flow acceleration in reducing the net production of turbulent kinetic energy is given by a ratio of the two terms in Eq. (14):

$$\chi = \frac{(\overline{u^2} - \overline{v^2}) \frac{\partial u}{\partial x}}{-\overline{u'v'} \frac{\partial u}{\partial y}} \qquad (15)$$

To establish the variation of χ in the flow direction requires a knowledge of the turbulent quantities across the boundary layer. In the absence of turbulence measurements in accelerated flows, this estimate is restricted to the flat-plate measurements of Klebanoff (Ref. 2) at a momentum thickness Reynolds number of about 8×10^3. The production term $-\overline{u'v'}\,\partial u/\partial y$ is largest in the wall vicinity where $(y\sqrt{\tau_w/\rho_e})/\nu_e \simeq 30$. Using the "law of the wall," Eq. (7), the velocity gradient is

$$\frac{\partial u}{\partial y} = \frac{2.5}{30} \frac{\tau_w}{\rho_e \nu_e}$$

An average value of $(\overline{u^2} - \overline{v^2})/(-\overline{u'v'}) \simeq 1.8$ is taken from Klebanoff's data since this ratio did not vary appreciably across most of the boundary layer. Approximating the velocity gradient $\partial u/\partial x$ by its free-stream value du_e/dx and combining the other approximations gives

$$\chi \simeq \frac{22\nu_e \dfrac{du_e}{dx}}{\dfrac{\tau_{w0}}{\rho_e}} \qquad (15b)$$

Although the constant 22 is somewhat arbitrary, the essential feature is the dependence of χ on the group

$$\frac{\nu_e \dfrac{du_e}{dx}}{\dfrac{\tau_{w0}}{\rho_e}}$$

The variation of χ along the nozzle is shown in Fig. 19 at $T_t = 1500°R$ for the range of stagnation pressures from 45 to 254 psia. With decreasing stagnation pressure, the increasing values of χ indicate the predicted reduced net production of turbulent kinetic energy. At the lowest stagnation pressure, χ attains a maximum value of 0.14. Actually, for the low stagnation pressures, the values of χ should exceed those shown, since the low heat transfer implies that the wall shear is below the predicted value. The variation of χ along the nozzle displays the same trend of being largest in the convergent section before diminishing through the throat and divergent section as the heat-transfer data at the low stagnation pressures which depart from those typical of a turbulent boundary

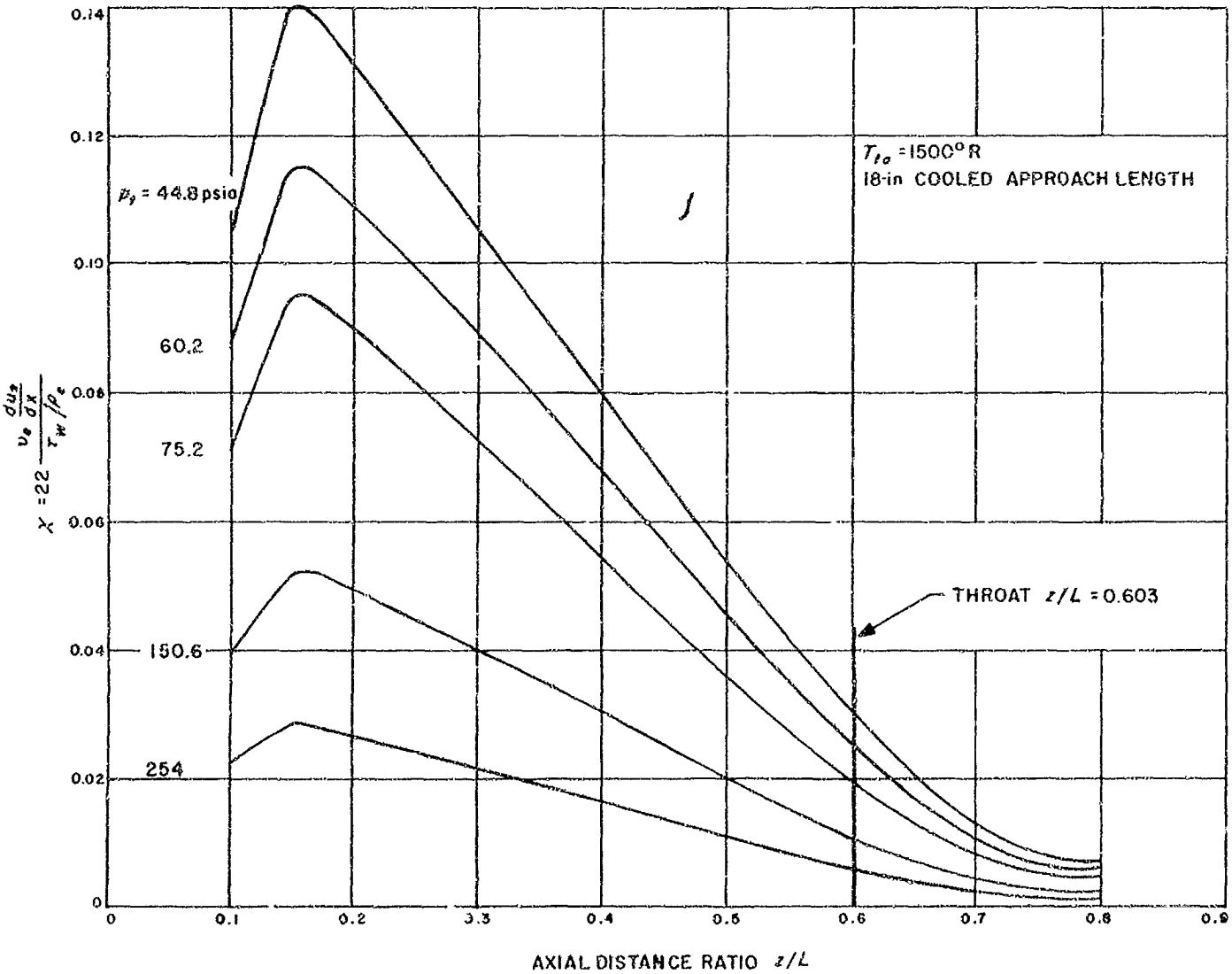

Fig. 19. Predicted effect of flow acceleration in reducing net production of turbulent kinetic energy at different stagnation pressures

layer observed in Fig. 12. The values of χ indicate when the turbulent shear stress $\overline{u'v'}$, which is related to the turbulent kinetic energy, is expected to be lower than that typical of a fully turbulent boundary layer. Th transport of heat would also be reduced, since it depend on the level of turbulent transport.

IX. CONCLUSIONS

Experimental convective heat-transfer results have been presented for a turbulent boundary-layer flow through a cooled convergent–divergent nozzle. The scope of the investigation covered a wide range of stagnation pressures and temperatures as well as nozzle-inlet boundary-layer thicknesses. The experimental results indicated the following:

1. Heat-transfer coefficients increased with increasing stagnation pressure as a result of the larger mass fluxes, but only at stagnation pressures above about 75 psia were values typical of a turbulent boundary layer.
2. At low stagnation pressures, the heat-transfer coefficients were below that typical of a turbulent boundary layer even though the boundary layers at the nozzle inlet were turbulent.
3. The effect of stagnation temperature on heat transfer was less clear, with the trends dependent on stagnation pressure.
4. Heat-transfer coefficients were about 10% higher throughout the nozzle with the thinnest boundary layer at the nozzle inlet ($\delta/R \simeq 0.05$) than with the thickest inlet boundary layer ($\delta/R \simeq 0.25$).
5. The heat-transfer coefficient is a maximum upstream of the throat, where the mass flux, deduced from wall static pressure measurements, is largest. Deviations of the mass flux from that predicted for one-dimensional flow amounted to as much as 15 just downstream of the throat.
6. A substantial decrease in heat transfer existed dow stream of the point of flow separation. Flow separ tion in the divergent portion of the nozzle occurr at the low stagnation pressures.

Various heat-transfer predictions were compared to t data. Fair agreement at the higher stagnation pressures provided by a modification of the turbulent boundar layer analysis of Ref. 15, in which the Stanton number taken dependent on a Reynolds number based on a thic ness characteristic of the thermal boundary layer. In t prediction, properties were evaluated at the free-stre temperature. For the low stagnation pressures, where t turbulent boundary layer is thought to have undergo partial transition toward a laminar one, a parameter found which is a measure of the importance of flow acc eration in reducing the transport of heat below that ty cal of a fully turbulent boundary layer.

More work is needed to gain some experimental kno edge of the flow an[3] thermal boundary layers within convergent–divergent nozzle and of the extent to wh these are predictable by an analysis such as that of [11]. To obtain this information, a conical nozzle of 10- half-angles of convergence and divergence has been c structed. This nozzle, which will be tested in the n future, is instrumented with boundary-layer probes incorporates the calorimetric technique to obtain he transfer measurements.

NOMENCLATURE

a speed of sound

A local nozzle cross-sectional area

A^* nozzle-throat area

c^* characteristic velocity of $\rho_0 A^* g_c / \dot{m}$

c_f local wall friction coefficient, $c_f/2 = \tau_w/\rho_e u_e^2$

c_f^* coefficient analogous to skin-friction coefficient, with momentum thickness dependence replaced by energy thickness

c_p specific heat at constant pressure

D nozzle diameter

D^* nozzle-throat diameter

g_c gravitational constant

h convective heat-transfer coefficient

k thermal conductivity

l cooled approach length

L axial length of nozzle = 5.925 in.

$\dot{m}$ mass flow rate

M Mach number

p static pressure

p_t stagnation pressure

Pr Prandtl number

q_w wall heat flux

$q^2/2$ turbulent kinetic energy

r nozzle radius

r^* nozzle-throat radius

r_c nozzle-throat radius of curvature

R nozzle-inlet radius = 2.53 in.

Re_D Reynolds number based on nozzle diameter, $\rho_e u_e D/\mu_e$

St Stanton number, $h/\rho_e u_e c_{p_e}$

T temperature

u velocity component in x-direction

u^+ dimensionless velocity, $u/\sqrt{\tau_w/\rho_e}$

v velocity component normal to wall

x distance along wall in flow direction

NOMENCLATURE (Cont'd)

y distance normal to wall

y^* dimensionless distance, $\dfrac{y\sqrt{\dfrac{\tau_w}{\rho_e}}}{\nu_e}$

z axial distance from nozzle inlet

γ specific-heat ratio

δ velocity boundary-layer thickness

δ_t stagnation-temperature boundary-layer thickness

δ^* displacement thickness

θ momentum thickness

μ viscosity

ν kinematic viscosity

ρ density

σ dimensionless property correction factor (defined in Ref. 22)

τ_w wall shear stress

ϕ energy thickness

χ parameter

Subscripts

a condition at radius which is less than r_b

aw adiabatic wall condition

b condition at radius which is greater than r_a

e condition at free-stream edge of boundary layer

f property evaluated at film temperature, $T_f = (T_w + T_e)/2$

i, j components in Cartesian coordinates

o upstream reservoir condition

t stagnation condition

w wall condition

1 one-dimensional flow value

Superscripts

$'$ fluctuating component

$\overline{\quad}$ time average

REFERENCES

1. Witte, A. B., and E. Y. Harper, *Experimental Investigation of Heat Transfer Rates in Rocket Thrust Chambers*, Technical Report No. 32-244, Jet Propulsion Laboratory, Pasadena, California, March 19, 1962. Also AIAA, Vol. 1, No. 2, 1963, pp. 443–51.

2. Saunders, O. A., and P. H. Calder, "Some Experiments on the Heat Transfer from a Gas Flowing Through a Convergent–Divergent Nozzle," *Proceedings of the 1951 Heat Transfer and Fluid Mechanics Institute*, Stanford University Press, 1951.

3. Rugsdale, W. C., and J. M. Smith, "Heat Transfer in Nozzles," *Chem. Engr. Sci.*, Vol. 11, 1960, p. 242–51.

4. Baron, J. R., and F. H. Durgin, *An Experimental Investigation of Heat Transfer at the Boundaries of Supersonic Nozzles*, Naval Supersonic Laboratory, Massachusetts Institute of Technology, WADC Technical Report 54-541, December 1954.

5. *Combined Bimonthly Summary No. 63, December 1, 1957 to February 1, 1958*, Jet Propulsion Laboratory, Pasadena, February 15 1958, pp. 28–30. *Combined Bimonthly Summary No. 65, April 1, 1958 to June 1, 1958*, Jet Propulsion Laboratory, Pasadena, June 15, 1958, p. 32.

6. Kolozsi, J. J., *An Investigation of Heat Transfer Through the Turbulent Boundary Layer in an Axially Symmetric, Convergent–Divergent Nozzle*, Aerodynamic Lab., Ohio State University, TM-8, July 1958.

7. Livesey, J. L., "The Behavior of Transverse Cylindrical and Forward-Facing Pressure Probes in Transverse Total Pressure Gradients," *Journal of the Aeronautical Sciences*, Vol. 23, October 1956, pp. 949–55.

8. Seban, R. A., and D. Doughty, *Heat Transfer to Laminar and Turbulent Boundary Layers with Constant and Variable Free-Stream Velocity*, University of California, Institute of Engineering Research, Series 41, No. 13, August 1954.

9. Oswatitsch, K., and W. Rothstein, *Flow Pattern in a Converging–Diverging Nozzle*, NACA TM-1215, March 1949.

10. Coles, D., "The Law of the Wake in the Turbulent Boundary Layer," *Journal of Fluid Mechanics*, Vol. 1, 1956, pp. 191–226.

11. Elliott, D. G., D. R. Bartz, S. Silver, *Calculation of Turbulent Boundary-Layer Growth and Heat Transfer in Axi-Symmetric Nozzles*, Technical Report No. 32-387, Jet Propulsion Laboratory, Pasadena, February 15, 1963.

12. Keenan, J. H., and J. Kaye, *Gas Tables*, Wiley and Sons, Inc., New York, 1956.

13. Sergienko, A. A., and V. K. Gretsov, "Transition from a Turbulent into a Laminar Boundary Layer," *Soviet Physics—Doklady*, Vol. 4, No. 2, October 1959, pp. 275–76.

14. Back, L. H., *Heat Transfer to Turbulent Boundary Layers with a Variable Free-Stream Velocity*, Ph.D. Thesis, University of California, Berkeley, California, June 1962.

15. Bartz, D. R., "An Approximate Solution of Compressible Turbulent Boundary-Layer Development and Convective Heat Transfer in Convergent–Divergent Nozzles," *Transactions of the ASME*, Vol. 77, No. 8, 1955, pp. 1235–45.

16. Reshotko, E., and M. Tucker, *Approximate Calculation of the Compressible Turbulent Boundary Layer with Heat Transfer and Arbitrary Pressure Gradient*, NACA TN-4154, 1957.

REFERENCES (Cont'd)

17. Seban, R. A., and H. W. Chan, *Heat Transfer to Boundary Layers with Pressure Gradients*, University of California, Institute of Engineering Research, Series 41, No. 16, July 1957.

18. McCarthy, T. F., *Heat Transfer to Turbulent Boundary Layers with a Pressure Gradient*, Master's Thesis, University of Minnesota, August 1960.

19. Coles, D. E., *The Turbulent Boundary Layer in a Compressible Fluid*, Report No. P-2417, The Rand Corporation, Santa Monica, California, August 22, 1961.

20. Wolf, H., *The Experimental and Analytical Determination of the Heat Transfer Characteristics of Air and Carbon Dioxide in the Thermal Entrance Region of a Smooth Tube with Large Temperature Differences Between the Gas and the Tube Wall*, Ph.D. Thesis, Purdue University, Lafayette, Indiana, March 1958. Also *ASME Journal of Heat Transfer*, Vol. 81, November 1959, pp. 267–79.

21. Kutateladze, S. S., and A. I. Leontev, "Drag Law in a Turbulent Flow of a Compressible Gas and the Method of Calculating Friction and Heat Exchange," *Akademiya Nauk, Belorussk, S.S.R.*, Minsk, U.S.S.R., January 1961, pp. 1–23, 23–27, translated and issued by Technical Information and Library Services, Ministry of Aviation, December 1961.

22. Bartz, D. R., "A Simple Equation for Rapid Estimation of Rocket Nozzle Convective Heat-Transfer Coefficients," *Jet Propulsion*, Vol. 27, January 1957, pp. 49–51.

23. Preston, J. H., "The Minimum Reynolds Number for a Turbulent Boundary Layer and the Selection of a Transition Device," *Journal of Fluid Mechanics*, Vol. 3, Part 4, January 1958, pp. 373–84.

24. Hinze, J. O., *Turbulence*, p. 62, McGraw-Hill Book Company, Inc., New York, New York, 1959.

25. Klebanoff, P. S., *Characteristics of Turbulence in a Boundary Layer with Zero Pressure Gradient*, NACA TN-3178, 1954.

APPENDIX

Construction and Calibration of Thermocouple Plugs

The thermocouples embedded in the 0.25-in.-diameter plugs were formed by welding the exposed ends of 0.005-in.-diameter fiberglass-insulated chromel and alumel wires to the bottoms of opposing radial holes, as shown in Fig. 3. The wires were injected into these holes by using a spring-loaded jig, and the junction weld was made on contact between the wire and the plug. The chromel and the alumel junctions were separated by approximately 0.0055 in. of plug material. The wires were then cemented into the grooves in the sides of the plugs with Technical G Copper Cement and calibrated. A finished plug is shown in Fig. A-1.

To provide good contact between surfaces when the plugs were pressed into the nozzle, both the surfaces of the plugs and the holes were finished to roughnesses less than 16 μin. An interference fit of 0.0005 in. between the plug and nozzle hole diameters was used. After the plugs were pressed into position flush with the outer surface of the nozzle, the inner ends were machined to match the contour of the nozzle. The locations at which the wires protruded from the outer ends of the plugs were sealed with Technical C Copper Cement, and a coat of Echo Bond 56-C conductive cement was applied over the plug and extended over the nozzle to exclude any possibility of water seepage into the plugs. The nozzle, after installation of plugs, is shown in Fig. A-2.

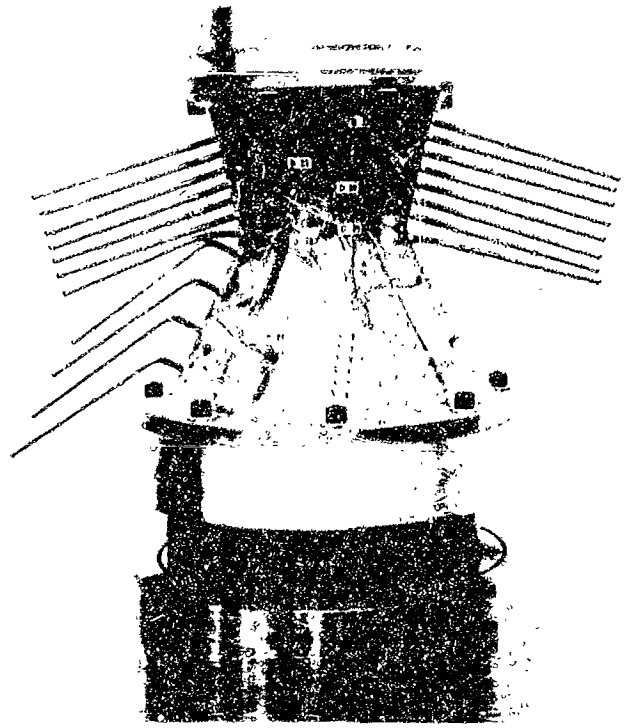

Fig. A-2. Nozzle after installation of thermocouple plugs

Fig. A-1. Thermocouple plug

For the calculation of the wall heat flux from Eq. (1), it is necessary to know precisely the distance between thermocouple weld junctions. Since the radial holes in the plugs were about three times the diameter of the bare end of the thermocouple wire, the exact location of the weld junction could not be obtained by physical measurement; thus, a Kelvin bridge circuit electrical calibrating technique was used as shown in Fig. A-3. This calibration was performed before the plugs were installed in the nozzle. A rod having the same diameter as a plug and of known electrical resistance R_R was connected to variable resistors R_b and R_d by wires with known resistances R_B and R_D. The plug with the thermocouples which were to be measured was held coaxially against one end of the rod. The contact resistance between rod and plug is represented by R_1. A thermocouple wire of unknown resistance R_c leading to one of the junctions was con-

APPENDIX (Cont'd)

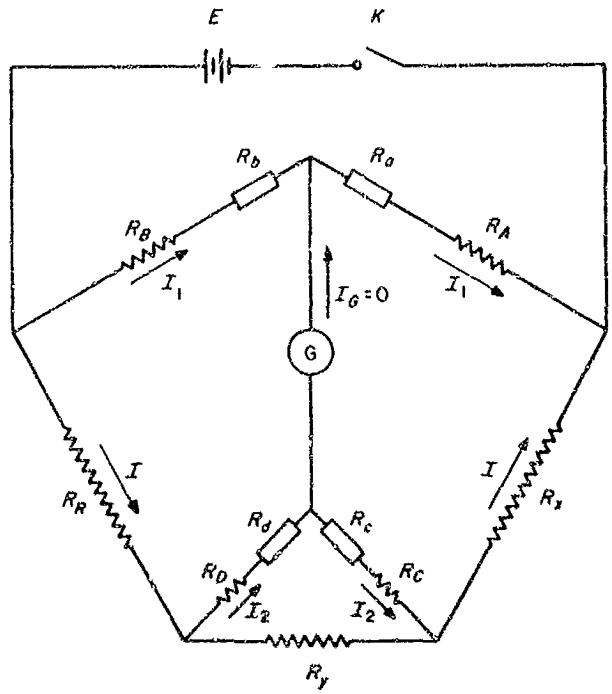

Fig. A-3. Kelvin bridge circuit used to determine thermocouple locations

nected to a variable resistor R_c and a galvanometer G. A thermocouple wire of the same material leading from another junction within the plug and represented by the unknown resistance R_A was connected to another variable resistor R_a, which was in turn connected to R_b and the other side of G. The resistance R_x represents the resistance of the plug between the junction wires R_c and R_A. The circuit assembly was completed with a battery E and a switch K. For the branch circuits with no current passing through G, Kirchkoff's second law may be applied, and the following equations may be written:

$$I_1 (R_A + R_a) = I_2 (R_C + R_c) + IR_x \qquad \text{(A-1)}$$

$$I_1 (R_B + R_b) = I_2 (R_D + R_d) + IR_R \qquad \text{(A-2)}$$

$$I_2 (R_C + R_c + R_D + R_d) = (I - I_2) R_y \qquad \text{(A-3)}$$

For $I_G = 0$,

$$\frac{R_A + R_a}{R_B + R_b} = \frac{R_C + R_c}{R_D + R_d} \qquad \text{(A-4)}$$

and the simultaneous solution of the above equatio (A-1–A-4) yields

$$R_x = R_R \frac{R_A + R_a}{R_B + R_b} \qquad \text{(A-}$$

Therefore, by proper adjustment of the resistances of t decade boxes such that $I_G = 0$, R_x is independent of t unknown contact resistance R_y. Actually, it was not p sible to make I_G exactly zero because of the limited sen tivity of the galvanometer; hence, R_y was made small comparison to R_x. Incorporating the following equatic using the electrical resistivity ρ,

$$R_x = \frac{\rho_x l_x}{A_x} \qquad \text{(A-}$$

$$R_R = \frac{\rho_R l_R}{A_R} \qquad \text{(A}$$

where l_R is the known length of the rod. Since the dia eters of the rod and plug are identical, $A_x = A_R$, solution of Eqs. (A-5), (A-6), and (A-7) yields

$$l_x = \frac{R_A + R_a}{R_B + R_b} l_R \frac{\rho_R}{\rho_x} \qquad \text{(}$$

Equation (A-8) was used to determine the dista between the junctions formed by two wires of the sa thermocouple material. The arithmetic average of tances between junctions formed by corresponding mel and chromel wires was then used as the dista between two thermocouple junctions.

The distance between the nozzle gas-side wall and inner thermocouple weld junction needed to calcu the wall temperature, however, could not be determi by the electrical technique and, consequently, had to measured physically. The distance from the radial h in which the inner thermocouple was welded to the in surface of the plug was measured before injection of wires. The length of the plug after installation and chining then made possible a simple calculation of distance from wall to inner thermocouple with the sumption that the thermocouple wires were locate the centerlines of the holes.

APPENDIX (Cont'd)

The estimated maximum total error that could have occurred in reported experimental values of heat-transfer coefficient in the throat region at the higher stagnation pressures and temperatures is approximately ±8%. This error results from a ±1% error due to thermocouple locations determined by the Kelvin bridge measurements, a ±1½% error from inaccuracies in measurement of the temperatures within the nozzle wall, a ±5% uncertainty in the difference between stagnation temperature and gas-side walls temperature, and a ±½% error from additional miscellaneous sources. Under conditions for which the temperature differences between adjacent thermocouples were the smallest such as at low stagnation pressure and temperature near the nozzle inlet, the maximum total error could have been as much as ±21%. It should be noted, however, that these are considered to be maximum errors and that the accuracy of the reported results is probably much better.

ACKNOWLEDGMENT

The authors express their gratitude to Donald R. Bartz, who initiated the project, designed the nozzle, and developed the method for accurately locating the thermocouple positions. Appreciation is extended to Kenton MacDavid for the installation of the thermocouples and calibration of the thermocouple plugs; Rod MacLean, who followed construction, installed and performed initial tests on the nozzle; Arthur Giggar for constructing boundary layer probes; Joe Godley and others for their significant contributions to the success of the project.